ACTA MEDICA (HRADEC KRÁLOVÉ)

2015, Vol. 58, No. 3

CONTENTS

REVIEW ARTICLE

MEG AS A MEDICAL DIAGNOSTIC TOOL IN THE GREEK POPULATION

Photios Anninos, Adam Adamopoulos, Athanasia Kotini

Lab of Medical Physics, Medical School, Democritus University of Thrace, Alexandroupolis, Greece

Summary: Magnetoencephalography (MEG) is the recording of the magnetic field produced by the flowing of ions in the brain. This article reports our experience in the application of MEG in patients and healthy volunteers in the Greek population. We provide a brief description of our research work. The MEG data were recorded in a magnetically shielded room with a whole-head 122 channel or an one-channel biomagnetometer. Our results lead us to believe that the MEG is an important research field which is evolving quickly with a number of interesting findings with respect to normal and abnormal functions of the human brain. It could provide clinical practice with an easy to perform non invasive method, which could be adjunct to conventional methods for the evaluation of brain disorders.

Keywords: *MEG; SQUID; Epilepsy; Febrile seizures; Parkinson; Multiple sclerosis; Alzheimer*

Introduction

Magnetoencephalography (MEG) is a noninvasive imaging technique, applicable to the human brain with a temporal resolution of approximately ~1 ms. In MEG, weak magnetic fields generated by electric currents in the brain are measured using Superconducting Quantum Interference Devices (SQUIDs) positioned on the skull. Time varying electric currents, in wires or brain cells, produce time-varying magnetic fields. Even though transmembrane, intracellular and extracellular neuronal currents each produce a surrounding magnetic flux, the neuromagnetic field recordable outside of the head is a selective reflection of intracellular currents flowing in the apical dendrites of pyramidal cells oriented parallel to the skull surface. This is a result of the biophysical properties of the neuronal currents and the volume conduction properties of the head. The output of each channel of the biomagnetometer is a time varying voltage waveform that reflects local changes in magnetic flux as a function of time. MEG is one of the non-invasive functional brain imaging techniques. Analysis of brain function by fMRI and PET is based on the change of cerebral blood flow induced by neural activity and that of EEG and MEG on the electric potential and magnetic changes induced by neural activity, respectively. Consequently, EEG and MEG feature higher temporal resolutions than PET and fMRI in measurements of brain activity.

In addition external transcranial magnetic stimulation (TMS) was applied to patients with CNS disorders with proper characteristics (magnetic field in the order of pT and frequency the alpha rhythm of the patient (8–13 Hz). The MEG recordings after the application of TMS shown a rapid attenuation of the abnormal MEG activity followed by an increase of the low frequency components and the alpha rhythm of the patients. Further signal analysis indicated that the application of the TMS strongly influenced the underlying brain dynamics with beneficial effects on the clinical status of the patients with CNS disorders.

This article reports our research work dealing with MEG as a diagnostic tool in medicine and its use in conjunction with other stimulation and theoretical methods for the evaluation of various diseases.

Methods

We employed the one-channel MEG system in 1985 and the 122-channel MEG system in 1999 from Greek Research programs. The 122-channel system provides a helmet shaped detector array covering the entire head allowing simultaneous recording of magnetic fields over the whole cortex and have a lot of advantages over the one-channel system.

A. 122-channel MEG system

The MEG recordings were carried out in a magnetically shielded room with a whole head 122-channel biomagnetometer (model: Neuromag-122, Helsinki, Finland) (Figure 1). During the recordings the subject was sitting in a chair with his/her head covered by the helmet-shaped dewar. The MEG sampling frequency was 256 Hz and the associated Nyquist frequency was 128 Hz, which was well above of the constituent frequency components of interest in our MEG recordings, thus avoiding aliasing artefacts. The time taken for each MEG recording was 3 min. For each MEG spike, we calculated the single equivalent current dipole (ECD) source at the spike peak. It was suitable for our measurements regarding localization of epileptic foci. We defined acceptable

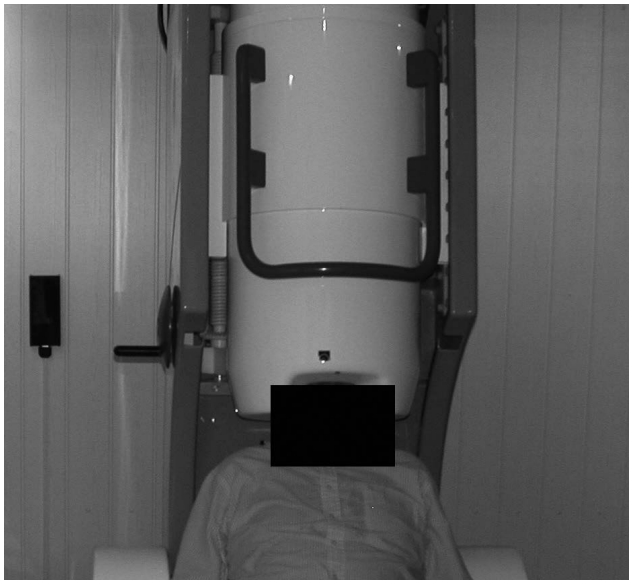

Fig. 1: The 122-channel MEG system with the patient during the measurements.

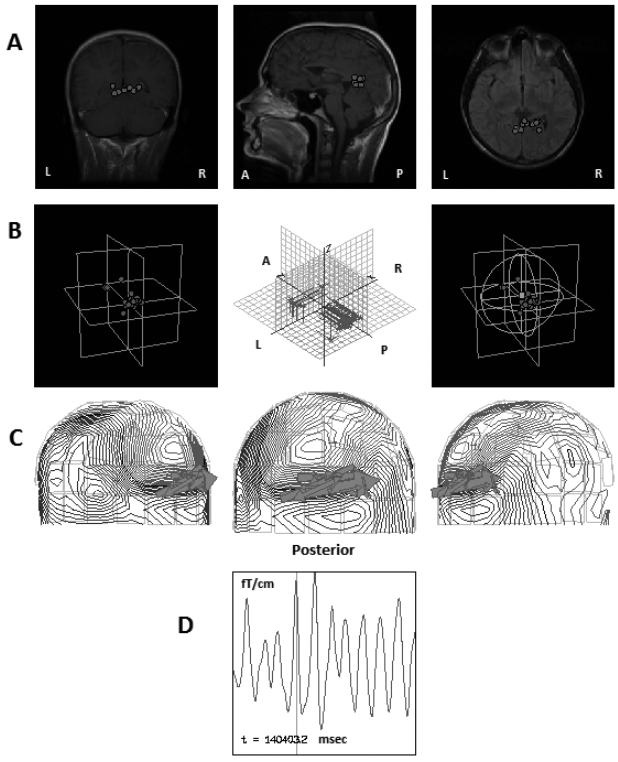

Fig. 2: A) Coronal, sagittal and axial MRI images for one patient with the superposition of the active ECDs indicated by the red dots. (L: left, R: right, A: anterior, P: posterior) B) The whole number of dipoles in the x, y, z axes. C) The scalp isocontour filed distribution and the ECDs indicated by the green arrows. D) The MEG raw data for a time duration where the ECDs were specified. The x axis is the time in msec and the y axis is the magnetic field in fT/cm (fT = femto Tesla).

ECDs as those with a goodness-of-fit to the model of >70% and with ECD strength between 100 and 400 nAm (nano Ampere metre). Three fiducial points were defined on each patient's head surface which were clear anatomic landmarks (the 2 preauricular points and the nasion). These 3 points define the coordinate system that includes the brain and the position of the magnetometers relative to it. The line between the preauricular points defines the x-axis of the coordinate system, with the positive direction being to the right. The line between the nasion and the mid-point of the x-axis and perpendicular to it, defines the y-axis and the line perpendicular to the x-y plane, passing through the intersection of the x and y-axes, defines the z-axis of the coordinate system. The positive y-axis passed through the nasion and the z-axis pointed upwards. The locations of the ECDs were estimated and projected onto the structural images of the brain (MRI), that displays the activated brain regions (Figure 2).

B. One-channel MEG system

Biomagnetic measurements were performed using a one channel second order gradiometer SQUID model 601 of the Biomagnetic Technologies Inc. (Figure 3), which was located in an electrically shielded room. The MEG recordings were performed after positioning the SQUID sensor 3 mm above the scalp of the patient, with the use of an optic positioning system, which was based on the International 10–20 Electrode Placement System. This system uses any one of the standard EEG recording positions as its origin. We used the P3, P4, T3, T4, F3 and F4 recording positions. The reference system was devised to retrieve maximal information from a specified area of the skull given that the gradiometer coil is theoretically equally sensitive to all magnetic flux lines perpendicular to a circular area of the brain. In our case, this circle has been an effective diameter of 2.36 cm, i.e. the diameter of the SQUID sensor coil. A rectangular 32-point matrix was used around the origin (4 rows × 8 columns, equidistantly spaced in a 4.5 cm × 10.5 cm rectangle) for positioning of the SQUID. The MEG was recorded from each cerebral hemisphere at each of the 32 matrix points on the scalp for 32 consecutive epochs. Each epoch was of 1 sec duration and was digitized with a sampling frequency of 256 Hz. The MEG signal was band-pass filtered with cut-off frequencies of 0.1 and 60 Hz. The MEG recordings were digitized using a 12 bit precision analog to digital converter with a sampling frequency of 256 Hz, and were stored in a PC peripheral memory for off-line Fourier statistical analysis. With this technique we obtained two dimensional isocontour spectral amplitude maps (ISO-SA maps) (Figure 4). These maps were useful in obtaining clearly defined areas of high spectral density in the 2–7 Hz band frequencies. In addition they were helpful in providing clear identification of the coordinates of the point on the scalp where the MEG power spectrum has its maximal power as well as its maximal magnetic field intensity. We investigated the 2–7 Hz frequency band because we were interested in

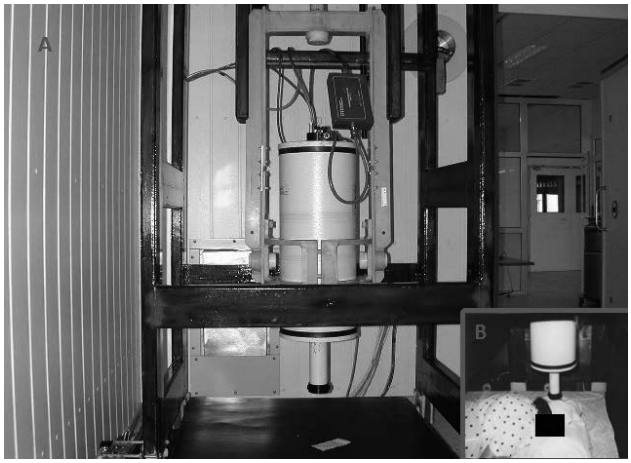

Fig. 3: A) The one-channel MEG system. B) The patient during the measurement.

the behavior of delta and theta rhythms. Figure 4 shows the left temporal lobe of an epileptic patient before and after the application of TMS. We observe a significant reduction of the magnetic field in the spectral amplitude maps after the application of TMS.

Results

A. 122-channel MEG system

Gustatory states

Gemousakakis et al. (1) evaluated MEG recordings for healthy female volunteers, in five different gustatory states: normal, sweet, bitter, sour and salty in all studied states. There was a higher number of low frequencies and a lower number of high frequencies with increasing age. Statistically significant differences were found in the normal and sweet states for the frequencies of 2 Hz and 7 Hz and in the salty taste in the frequency of 7 Hz. They also intra-compared the five states in group A and the five states in group B for the 2 Hz and 7 Hz frequencies. The results were not statistically significant.

Gemousakakis et al. (2) evaluated MEG recordings in five different states: normal condition, sweet, bitter, sour, and salty taste. The results showed that, in the normal condition, as well as in the sweet and the bitter taste, the male volunteers exhibited a higher count of low-frequency than high-frequency channels compared to the female ones; in the case of the sour taste, there was no clear differentiation between the genders; for the salty taste, the female volunteers exhibited a higher number of low-frequency channels whereas there was no clear differentiation in the number of high frequencies between the gender.

Anninos et al. (3) investigated the localization of current sources for spontaneous MEG data in the frequency domain. MEGs were evaluated in three different states: physiological, sweet and salty. Low frequencies can be seen in the maps obtained with the sweet taste, whereas in the physiological and salty taste, the maps showed higher frequencies in the majority of channels.

Epilepsy

Antoniou et al. (4) revealed quantitative differences in the MEG received from patients with Idiopathic Generalized Epilepsy (IGE) and from healthy volunteers. The analysis demonstrated the existence of spatially diffused low dimensionality in the MEG signals of patients with IGE.

Kotini et al. (5) investigated the electromagnetic sources of epileptic activity in two patients with juvenile myoclonus epilepsy (JME). The MRI examinations for both patients did not disclose any focal lesions or areas of abnormal signal intensity or enhancement by contrast media. MEG was recorded 5 years after the disease onset for the first patient and 11 years for the second patient. For the first patient dipolar sources of MEG paroxysmal activity were localized at the vermis and extending up to the occipital region, whereas,

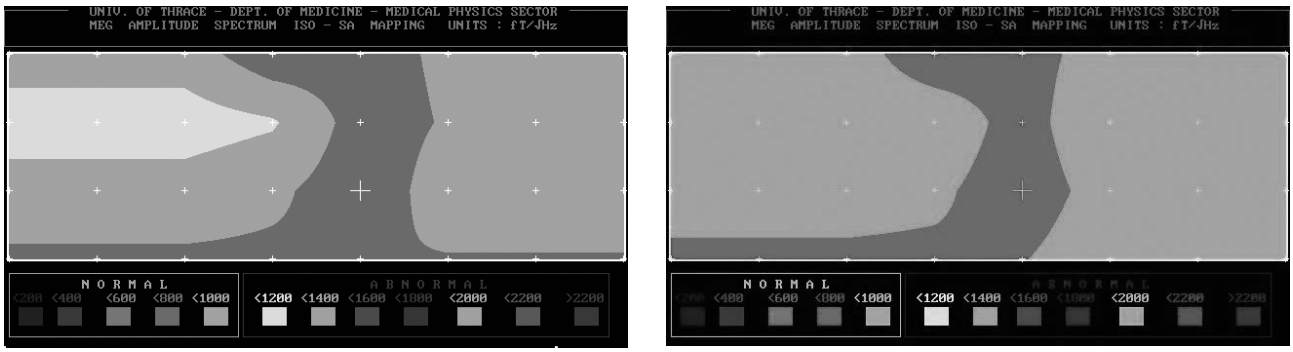

Fig. 4: The ISO-SA map of the left temporal area of an epileptic patient A) before and B) after the application of TMS. The large symbol "+" represents the reference point for the left hemisphere for easy identification of the coordinates of the functional focal points. The white small symbols "+" represent the 32 measured points with respect to the reference points. The maximal total average emitted power in the 2–7 Hz frequency band was >1000 fT/√Hz before TMS and became <1000 fT/√Hz afterwards.

for the second patient dipolar sources of MEG paroxysmal activity were localized at the cerebellar area (vermis and hemisphere).

Anninos et al. (6) assessed any cerebral dysfunction in young children, who experienced febrile seizures, by means of MEG. ECDs were calculated for epileptic spikes on MEG recordings according to the ECD. Of 15 children, 8 showed ECDs located at the left-temporal, right-temporal, occipital, and frontal lobe, as active regions responsible for febrile seizures. They assumed that the interictal epileptiform discharges were a consequence of febrile seizures.

Kotini et al. (7) investigated the localization of current sources from spontaneous MEG data recorded from epileptic patients randomly selected, with different types of epilepsy. For each MEG spike, they calculated the ECD sources at the initial spike peaks with a spherical model. For each patient there was an increase of the frequency range after the ECD in compared to the one before the ECD. This was present in the whole study group due to epileptic discharge which was statistically significant. There was also a statistically significant difference in the increase of the frequency range in four patients with pathologic MRI, in five patients with normal MRI, in five patients with a high incidence of seizures and in four patients with onset age < 10 years.

Alzheimer Disease

Abatzoglou et al. (8) obtained MEG from Alzheimer Disease (AD) patients and analyzed them using Fourier Transform in order to get the frequency distribution of MEG values. From this evaluation it was concluded that in patients with AD the dominant frequencies were significantly lower compared to normal individuals.

Transcranial Magnetic Stimulation (TMS)

TMS and CNS Disorders

Anninos et al. (9) applied external transcranial magnetic stimulation (TMS) to patients with proper characteristics which were obtained with MEG recordings prior to TMS. The MEG recordings after the application of TMS showed a rapid attenuation of the high abnormal activity followed by an increase in the number of the low frequency components toward the patients alpha-rhythm. The possible mechanisms of the effects of TMS on the pineal gland in the brain were presented.

TMS and Parkinson Disease

Anninos et al. (10) applied TMS in the order of pico Tesla on the patients with proper field characteristics which were obtained prior to TMS. The patients responded to the TMS with a feeling of relaxation and partial or complete disappearance of tremor, muscular ache and levodopa induced dyskinesias as well as rapid reversed visuospatial impairment, which were followed by a corresponding improvement and normalization of the MEG.

Parkinson Disease

Kotini et al. (11) investigated the MEG recordings from PD patients and healthy volunteers in the frequency domain. Prominent low frequencies can be seen in the spectrum obtained from the PD patients. MRI did not disclose specific findings in any case.

Malignant CNS lesions

Antoniou et al. (12) presented recordings from 2 patients diagnosed with malignant CNS lesions. By applying the Grassberger-Procaccia method of phase space reconstruction to the MEG of patients with malignant CNS lesions they found clear evidence linking the embedding dimension m in which they had the onset of saturation with the progress of the treatment.

Antoniou et al. (13) investigated the MEG from patients with malignant CNS lesions and from healthy volunteers. Evidence linking MEG signal characteristics (existence of low dimensionality chaotic dynamics) with the existence of the tumour was found from this analysis.

B. One-channel MEG system

Alzheimer Disease

Abatzoglou et al. (14) applied non-linear analysis on MEG signals of Alzheimer Disease (AD) patients in order to investigate the underlying complexity of the brain dynamics. Some recorded points were found with high amplitudes and low frequencies in magnetic activity. By applying nonlinear analysis in these records, low values in the correlation dimension D of the reconstructed phase space were found.

Multiple sclerosis

Kotini et al. (15) investigated multiple sclerosis (MS) patients. Some of the recorded points were observed to exhibit abnormal rhythmic activity, characterized by lower amplitudes and frequencies compared with controls. Using the MEG brain activity they were able to obtain a mapping technique characterized by the spectral amplitude of scalp distribution.

Kotini et al. (16) investigated if there was any nonlinearity in the MEG recordings of patients with MS in comparison with controls in order to find out the differences in the mechanisms underlying their brain waves. Chaotic activity of MS patients was lower than in the normal brain.

Transcranial Magnetic Stimulation (TMS)

TMS and Arachnoid Cyst

Anninos et al. (17) reported a 34-year-old male diagnosed of an intracranial arachnoid cyst arising in the left-sided temporal-parietal area that underwent evaluation by means of

MEG. Biomagnetic waveform recordings were obtained from the target area and Fourier analysis of these measurements was carried out. External TMS in the order of pico Tesla was applied with proper field characteristics which were obtained prior to the application and the emitted MEG activity was recorded again. The cortical area adjacent to the borders of the arachnoid cyst emitted biomagnetic waveforms with high values. The application of TMS resulted in a rapid attenuation of the high MEG activity in the target area.

TMS and Epstein Barr

Anninos et al. (18) reported a 2-years-old male infant with a history of Epstein-Barr virus encephalitis, treated with foscarnet and steroids, because he developed mutism, ataxia and loss of the ability to eat, walk and talk. Brain imaging revealed loss of white matter around ventricles and progressive global brain atrophy, findings consistent with encephalopathy. There was an improvement of the clinical findings after the application of TMS with proper field characteristics. This case illustrated the possibility of therapeutic applications of TMS with proper field characteristics to normalize pathologically decreased levels of brain cortex activity.

TMS and Alopecia universalis

Anninos et al. (19) used MEG measurements and external magnetic field in the differential diagnosis and management of gynaecological and neurological entities. Exogenous TMS and MEG findings had been applied in the treatment of an alopecia universalis case. Important hair regrowth appeared progressively from the 2nd week till the 15th month of the therapeutic protocol. The indubitable superiority (comparatively to the control group) was noted.

TMS and Epilepsy

Anninos et al. (20) investigated the influence of external TMS in epileptic patients using MEG measurements and non-linear analytic techniques. In order to investigate the existence of any alteration in the complexity underlying the neural dynamics characterizing the pathologic brain before and after the TMS, a chaotic analysis approach was applied for the estimation of the dimensional analysis of the existing strange attractors. The application of TMS resulted in rapid attenuation of the MEG activity of epileptic patients. The obtained results of the dimensionality calculation provided a shift from lower to higher dimensional values, which is an indication that the system is chaotic.

Anninos et al. (21) presented three randomly selected epileptic patients in which application of external TMS of low intensities and frequencies produced a substantial attenuation of their abnormal brain activity. Furthermore, they presented a statistical analysis of 50 randomly selected epileptic patients who underwent TMS for the treatment of their seizures and they found that the anticonvulsant response to TMS was statistically significant.

Anninos et al. (22) measured the MEG from a patient with history of tonic-clonic seizures over 27 years who, despite medical treatment, experienced 8–10 convulsions daily. Subsequently, they energized an electronic device, which emitted magnetic fields with proper frequencies and intensities, and returned these back to the subject's brain. After magnetic stimulation with this electronic device, the seizures stopped.

Anninos et al. (23) developed a mapping technique using the MEG brain activity from epileptic patients. In addition by utilizing the characteristics of the Fourier power spectrum from the recorded MEG data they were also able to energize a magnetic stimulator which emits back to the patient's brain TMS with proper frequencies and intensities. Furthermore chaotic analysis approach was applied for the estimation of the dimensional analysis of the existing strange attractors. The obtained results of the dimensionality estimation furnish strong evidence of a shift of the correlation dimension to higher values after the application of TMS.

TMS and Parkinson Disease

Anninos et al. (24) obtained MEG recordings from patients suffering from Parkinson's disease (PD). External TMS was applied and the brain magnetic activity was recorded again. The application of TMS resulted in rapid attenuation of the MEG activity of PD patients. Furthermore, chaotic dynamic methods were used, in order to estimate the correlation dimension D of the reconstructed phase spaces. The estimated values of D, in conjunction with the results derived from the other data analysis methods, strongly supported the existence of low dimension chaotic structures in the dynamics of cortical activity of PD patients.

TMS and Multiple Sclerosis

Anninos et al. (25) used MEG recordings from MS patients and applied TMS back to the MS patients brain with proper frequencies and intensities. Furthermore they applied non-linear analysis in order to investigate if there was any alteration in the complexity underlying the dynamics, which characterized the brain of MS patients before and after TMS. The obtained results of the dimensionality estimation furnished a strong evidence of a shift of the correlation dimension to a higher value after the application of TMS.

TMS and Meniere Syndrome

Anninos et al. (26) investigated Meniere's syndrome. Using MEG they obtained the magnetic power spectrum distribution and utilizing its characteristics, they applied TMS back to the patient's brain. The brain activity was recorded and analyzed again, and by applying non-linear analysis they were able to investigate the brain's complexity. The results of the dimensionality estimation furnished a shift of the correlation dimension to higher values.

Theoretical model and Epilepsy

Kotini et al. (27) compared a theoretical neural net model with MEG data from epileptic patients and normal individ-

uals. Using the method of x^2-fitting it was found that the MEG amplitudes in epileptic patients and normal subjects had Poisson and Gauss distributions respectively. The Poisson connectivity derived from the theoretical neural model represented the state of epilepsy, whereas the Gauss connectivity represented normal behavior. The MEG data obtained from epileptic areas had higher amplitudes than the MEG from normal regions and were comparable with the theoretical magnetic fields from Poisson and Gauss distributions.

Anninos et al. (28) provided information from neural models on the role played by the specific anatomy of various brain centers in determining their function. The experimental approach proposed here involved a comparison between MEG in normal and epileptic patients and an analysis of model nerve net using computer stimulation in a large general-purpose digital computer.

Neonatal MEG

Kotini et al. (29) investigated the presence of any non-linearity in the MEG recordings in neonates born to preeclamptic pregnancies in comparison with the ones born to uncomplicated pregnancies, in order to find out the differences in the mechanisms underlying their brain waves. The above analysis of the MEG in neonatal preeclamptic brain exhibited a lower dimension complexity compared to the normal neonatal brain, as well as the first Lyapunov exponent, which mean lower information processing.

Anastasiadis et al. (30) performed a prospective study of neonatal brain function on respective term neonates who were delivered normally, without any clinical signs of brain damage. These MEGs were low in almost all neonates from the "normal pregnancy" group, while they were high in most neonates from the "pre-eclamptic" group. The difference between the two groups was statistically significant. A statistically significant difference in spectral amplitudes of neonatal brain activity was observed between normal term and pre-eclamptic neonates.

Shizophrenia

Kotini et al. (31) investigated the presence of any non-linearity in the MEG from the temporal lobe of schizophrenic patients in comparison with controls, in order to find the differences underlying the brain waves. There were no significant differences between the two groups as far as age and sex were concerned. The analysis of the MEG in the schizophrenic group exhibited lower dimension complexity. Moreover the first Lyapunov exponent showed lower values compared with the corresponding ones in the control group, which mean lower information processing.

Alzheimer

Anninos et al. (32) obtained MEG from the brain of patients suffering from AD. Furthermore, chaotic dynamic methods were used, in order to estimate the correlation dimension D of the reconstructed phase spaces. The estimated values of D, in conjunction with the results derived from the order data analysis methods, strongly supported the existence of low dimension chaotic structures in the dynamics of cortical activity of AD patients.

The TMS electronic device

The TMS electronic device is a modified helmet containing up to 122 coils which are arranged in five array groups, so as to cover the main 5 brain regions (frontal, vertex, right and left temporal and occipital regions) of the subject. It is designed to create TMS range modulations of magnetic flux in the alpha frequency range (8–13 Hz) of each patient. The TMS device was configured for each individual to generate a square wave (so as to resemble the firing activity of neurons in the brain) modulated magnetic field at the individual's mean peak alpha frequency (33, 34).

Discussion

The ionic currents which originate from biochemical sources at the cellular level in the CNS produce electric and magnetic fields. The generation of EEG signals in the brain, is an exact way to determine the potential distribution at the scalp given a set of intracerebral current sources. EEG can only be measured at a considerable distance from the source if the responsible neurons are regularly arranged and activated in a more or less synchronous way. Thus, while with the EEG it is very difficult to localize where a particular signal originates in the brain, in the case of the magnetic field it is easier to localize the signals origin in the brain. The MEG is presently regarded as the most efficient method for recording the brain activity in real time for many reasons.

Compared with the EEG, the MEG has unique sensitivity to the CNS disorders and normal functions of the brain. In addition, the MEG offers functional mapping information and measurement of brain activity in real time, unlike CT, MRI and fMRI which only provide structural, anatomical and metabolic information. With the MEG the brain is seen in 'action' rather than viewed as a still image. Another most important point is that the MEG has far more superior ability to resolve millisecond temporal activity associated with the processing of information which is the main task of our brain. Other properties of the MEG that should be mentioned are the following: Neither electrodes nor a reference point are necessary for recording the MEG compared to the EEG; the transducers for the MEG need not touch the scalp, because the magnetic field does not disappear where conductivity is zero. The recordings of the MEG are the measurements of the magnetic fields perpendicular to the skull, which are caused by tangential current sources. By contrast, the EEG is a measure of both components. This means MEG measures the cortical activity lying in the sulci and not in the convexity of the gyri (35–37). From the measured field, it is possible, by making appropriate assumptions, to calculate backwards

the activated brain area. In interpreting MEG data, one is dealing with the electromagnetic inverse problem, i.e., with the calculation of the source currents responsible for the measured extracranial magnetic field with the use of ECD. Matching an ECD model to the extracranial magnetic field became a simple and convenient method for localizing sources of cerebral activity. Experimental studies proved the accuracy of ECD localization of sources of interictal discharges (38–44).

The most important clinical results derived by the use of MEG are obtained from the preoperative examination of sources of epileptic activity and the surgical planning in patients with brain tumors. The knowledge of the position of the primary sensory areas and those involved in speech production and comprehension is a prerequisite for avoiding potential neurological deficits during the surgery (45–48). Source localization of MEG spikes is often performed in clinical practice for identifying an irritative zone. The source analysis of MEG signals incorporates anatomical information derived from the MRI with the sources of neural activities from each patient providing a current dipole distribution map. The ECD analysis has been widely used for source localization of epileptic spikes for decades. It assumes that a single dipole source generates all the neuromagnetic fields recorded from the sensors. Adequate ECDs are mapped on the patient's MRI (45, 46). It is a well established procedure with some limitations. The inverse problem localizes in three dimensional space the neural sources of the MEG recordings. Methods to solve the inverse problem need to make additional assumptions according to the experimental protocol. An alternative method to overcome the inverse problem is to use the beamforming (49). This method extracts the origins of a signal from a specified spatial location. MEG investigates also oscillatory brain activity by using Fourier, Wavelet or Hilbret transformations showing significant changes in the power and synchronization of the oscillatory activity (50).

The MEG spike morphology has not been adequately described while the EEG spikes were well defined. A clinical guideline has recommended indentifying the MEG spikes based on the principles established for EEG (51). The MEG spikes are useful for clinical application mostly in patients with negative EEG (46).

Consequently, the MEG could provide clinical practice with a non-invasive and rapid method, which could be adjunct to conventional methods for the assessment of brain dysfunction.

References

1. Gemousakakis T, Anninos P, Zissimopoulos A, et al. A study on the age dependency of gustatory states: Low-frequency spectral component in the resting-state MEG. J Integr Neurosci 2013; 12: 1–13.
2. Gemousakakis T, Kotini A, Anninos P, Zissimopoulos A, Prassopoulos P. MEG evaluation of taste by gender difference. J Integr Neurosci 2011; 10: 537–45.
3. Anninos P, Kotini A, Adamopoulos A, et al. Identification of taste quality with the use of MEG. J Integr Neurosci 2006; 5: 535–540.
4. Antoniou P, Adamopoulos A, Anninos PA, Piperidou H, Kotini, A. Assessing brain pathophysiology through non linear analysis of MEG in Idiopathic Generalized Epilepsy cases. J Behav Brain Sci 2012; 2: 445–453.
5. Kotini A, Mavraki E, Anninos P, Piperidou H, Prassopoulos P. Magnetoencephalographic findings in two cases of juvenile myoclonus epilepsy. Brain Topogr 2010; 23: 41–5.
6. Anninos P, Kotini A, Dipla V, Tsalkidis A, Chatsimichail A. MEG evaluation of Febrile Seizures in Young Children. J Child Neurol 2010; 25: 61–6.
7. Kotini A, Mavraki E, Anninos P, Piperidou H, Prassopoulos P. MEG evaluation of epileptic activity in the time and frequency domain. J Integr Neurosci 2008; 7: 463–80.
8. Abatzoglou I, Anninos P, Tsalafoutas I, Koukourakis M. Multi-channel magnetoencephalogram on Alzheimer disease patients. J Integr Neurosci 2009; 8: 13–22.
9. Anninos P, Kotini A, Anninou N, Adamopoulos, A, Papastergiou, A, Tsagas, N. MEG recordings of patients with CNS disorders before and after external magnetic stimulation. J Integr Neurosci 2008; 7: 17–27.
10. Anninos P, Adamopoulos A, Kotini A, Tsagas N, Tamiolakis D, Prassopoulos P. MEG evaluation of Parkinson's diseased patients after external magnetic stimulation. Acta Neurol Belg 2007; 107: 5–10.
11. Kotini A, Anninos P, Adamopoulos A, Prassopoulos P. Low Frequency MEG Activity and MRI Evaluation in Parkinson's Disease. Brain Topogr 2005; 18: 59–63.
12. Antoniou P, Anninos P, Piperidou H, et al. Treatment evaluation of brain tumors using non-linear analysis of Magnetoencephalographic data. A novel technique. Gazz Med Ital 2004; 163: 285–290.
13. Antoniou P, Anninos P, Piperidou H, et al. Non linear analysis of Magnetoencephalographic signals as a tool for assessing malignant lesions of the brain; first results. Brain Topogr 2004; 17: 117–123.
14. Abatzoglou I, Anninos P, Adamopoulos A, Koukourakis M. Nonlinear analysis of brain magnetoencephalographic activity in Alzheimer disease patients. Acta Neurol Belg 2007; 107: 34–9.
15. Kotini A, Anninos P, Tamiolakis D. MEG mapping in multiple sclerosis patients. Eura Medicophys 2007; 43: 345–8.
16. Kotini A, Anninos P, Tamiolakis D, Prassopoulos P. Differentiation of MEG activity in multiple sclerosis patients with the use of nonlinear analysis. J Integr Neurosci 2007; 6: 233–40.
17. Anninos P, Kotini A, Tamiolakis D, Prassopoulos P. Evaluation of an intracranial arachnoid cyst with MEG after external magnetic stimulation. J Integr Neurosci 2007; 6: 227–32.
18. Anninos P, Kotini A, Tamiolakis D, Tsagas N. Transcranial magnetic stimulation. A case report and review of the literature. Acta Neurol Belg 2006; 106: 26–30.
19. Anninos P, Karpouzis A, Kotini A, Kouskoukis C. Exogenous magnetic stimulation in therapeutic management of universalis alopecia areata. Gazz Med Ital 2004; 163: 281–284.
20. Anninos P, Kotini A, Adamopoulos A, Tsagas N. Magnetic stimulation can modulate seizures in epileptic patients. Brain Topogr 2003; 16: 57–64.
21. Anninos P, Tsagas N, Jacobson J, Kotini A. The biological effects of magnetic stimulation in epileptic patients. Panminerva Med 1999; 41: 207–15.
22. Anninos P, Tsagas N, Jacobson J, Kotini A. The biological effects of magnetic stimulation in epileptic patients. Review Series Neurology 2001; 2: 15–17.
23. Anninos P, Kotini A, Adamopoulos A, Tsagas N. The use of nonlinear analysis for differentiating brain biomagnetic activity in epileptic patients before and after magnetic stimulation. Hardronic J Suppl 1999; 14: 1–26.
24. Anninos P, Adamopoulos A, Kotini A, Tsagas N. Nonlinear Analysis of Brain Activity in Magnetic Influenced Parkinson Patients. Brain Topogr 2000; 13: 135–144.

25. Anninos P, Tsagas N, Kotini A, Adamopoulos A. The chaos theory for differentiating brain biomagnetic activity in normal and multiple sclerosis patients before and after magnetic stimulation. Hardronic J Suppl 1999; 14: 137–151.
26. Anninos P, Tsagas N, Kotini A, Konstantinopoulos, P. The use of nonlinear analysis for differentiating brain biomagnetic activity in normal and Meniere's syndrome patients before and after magnetic stimulation. Hardronic J Suppl 1999; 14: 153–170.
27. Kotini A, Anninos P, Anastasiadis AN, Tamiolakis D. A Comparative Study of a Theoretical Neural Net Model with MEG Data from Epileptic Patients and Normal Individuals. Theor Biol Med Model 2005; 2: 37.
28. Anninos P, Kotini A, Papastergiou A, Tsagas N. Neural Modeling approach to determine Structure and Function in Brain Center. Hardronic J Suppl 2000; 15: 154–184.
29. Kotini A, Koutlaki N,Anninos P, Adamopoulos A, Liberis V, Anastasiadis P. Chaotic analysis approach in neonatal MEG. Biol Neonate 2003; 84: 214–221.
30. Anastasiadis P, Anninos P, Koutlaki N, Kotini A, Avgidou K, Adamopoulos A. Neonatal MEG and spectral analysis. Clin Exp Obstet Gynecol 2001; 28: 269–273.
31. Kotini A, Anninos P. Detection of non-linearity in schizophrenic patients using MEG. Brain Topogr 2002; 15: 107–113.
32. Anninos P, Kotini A, Adamopoulos A, Tsagas N, Jacobson J. Nonlinear Analysis of MEG Activity Recorded in Alzheimer Patients. Hardronic J Suppl 2000; 15: 1–16.
33. Anninos PA, Tsagas N, Sandyk R, Derpapas K (1991) Magnetic stimulation in the treatment of partial seizures. Int J Neurosci 60: 141–171.
34. Anninos PA, Tsagas N (1995) Electronic apparatus for treating epileptic individuals. US patent 5453072 Sept 26.
35. Bast T, Wright T, Boor R, et al. Combined EEG and MEG analysis of early somatosensory evoked activity in children and adolescents with focal epilepsies. Clin Neurophysiol 2007; 118: 1721–35.
36. Ramantani G, Boor R, Paetau R, et al. MEG versus EEG: influence of background activity on interictal spike detection. J Clin Neurophysiol 2006; 23: 498–508.
37. Rodin E, Funke M, Berg P, Matsuo F. Magnetoencephalographic spikes not detected by conventional electroencephalography. Clin Neurophysiol 2004; 115: 2041–7.
38. Hamalainen M, Hari R, Ilmoniemi R, Knuutila J, Lounasmaa OV. Magnetoencephalography: theory, instrumentation, and applications to non-invasive studies of the working human brain. Rev Mod Phys 1993; 65: 413–497.
39. Ishii R, Canuet L, Aoki Y, et al. Frequency diversity of posterior oscillatory activity in human revealed by spatial filtered MEG. J Integr Neurosci 2013; 12: 343–53.
40. Iwaki S, Bonmassar G, Belliveau JW. Dynamic cortical activity during the perception of three-dimensional object shape from two-dimensional random-dot motion. J Integr Neurosci 2013; 12: 355–67.
41. Kishida K. Neurodynamics of somatosensory cortices studied by magnetoencephelography. J Integr Neurosci 2013; 12: 299–329.
42. Knowlton RC, Laxer KD, Aminoff MJ, Roberts TP, Wong ST, Rowley HA. Magnetoencephalography in partial epilepsy: clinical yield and localization accuracy. Ann Neurol 1997; 42: 622–631.
43. Oishi M, Kameyama S, Masuda H, et al. Single and multiple clusters of magnetoencephalographic dipoles in neocortical epilepsy: significance in characterizing the epileptogenic zone. Epilepsia 2006; 47: 355–364.
44. Tonoike M, Yoshida T, Sakuma H, Wang LQ. fMRI measurement of the integrative effects of visual and chemical senses stimuli in humans. J Integr Neurosci 2013; 12: 369–84.
45. Stufflebeam S. Clinical magnetoencephalography for neurosurgery. Neurosurg Clin N Am 2011; 22: 153–67.
46. Tanaka N, Stufflebeam S. Clinical application of spatiotemporal distributed source analysis in presurgical evaluation of epilepsy. Front Hum Neurosci 2014; 8: 62.
47. Dorfer C1, Widjaja E, Ochi A, Carter Snead Iii O, Rutka JT. Epilepsy surgery: recent advances in brain mapping, neuroimaging and surgical procedures. J Neurosurg Sci 2015 Jun; 59(2): 141–55.
48. Pizzella V, Marzetti L, Della Penna S, de Pasquale F, Zappasodi F, Romani GL. Magnetoencephalography in the study of brain dynamics. Funct Neurol 2014 Oct–Dec; 29(4): 241–53.
49. Woolrich M, Hunt L, Groves A, Barnes G. MEG beaforming using Bayesian PCA for adaptive data covariance matrix regularization. Neuroimage 2011; 57: 1466–79.
50. Proudfoot M, Woolrich MW, Nobre AC, Turner MR. Magnetoencephalography. Pract Neurol 2014 Oct; 14(5): 336–43.
51. Bagic, AI, Knowlton RC, Rose DF, Ebersole JS, ACMEGS Clinical Practice Guideline (CPG) Committee (2011). American clinical magnetoencephalography society clinical practice guideline 1: recording and analysis of spontaneous cerebral activity. J Clin Neurophysiol 2011; 28, 348–354.

Received: 26/03/2015
Accepted in revised form: 30/07/2015

Corresponding author:

Associate Professor A. Kotini, Lab of Medical Physics, Medical School, Democritus, University of Thrace, University Campus, 68100, Alexandroupolis, Greece; e-mail: akotini@med.duth.gr

ORIGINAL ARTICLE

CELL STRATIFICATION, SPHEROID FORMATION AND BIOSCAFFOLDS USED TO GROW CELLS IN THREE DIMENSIONAL CULTURES

Hana Hrebíková, Dana Čížková, Jana Chvátalová, Rishikaysh Pisal, Richard Adamčik, Pavel Beznoska, Daniel Díaz-Garcia, Jaroslav Mokrý

Department of Histology and Embryology, Charles University Medical Faculty, Hradec Králové, Czech Republic

Summary: The cell culture became an invaluable tool for studying cell behaviour, development, function, gene expression, toxicity of compounds and efficacy of novel drugs. Although most results were obtained from cell cultivation in two-dimensional (2D) systems, in which cells are grown in a monolayer, three-dimensional (3D) cultures are more promising as they correspond closely to the native arrangement of cells in living tissues. In our study, we focused on three types of 3D in vitro systems used for cultivation of one cell type. Cell morphology, their spatial distribution inside of resulting multicellular structures and changes in time were analysed with histological examination of samples harvested at different time periods. In multilayered cultures of WRL 68 hepatocytes grown on semipermeable membranes and non-passaged neurospheres generated by proliferation of neural progenitor cells, the cells were tightly apposed, showed features of cell differentiation but also cell death that was observable in short-term cultures. Biogenic scaffolds composed of extracellular matrix of the murine tibial anterior muscle were colonized with C2C12 myoblasts in vitro. The recellularized scaffolds did not reach high cell densities comparable with the former systems but supported well cell anchorage and migration without any signs of cell regression.

Keywords: *3D cell culture; Hepatocytes; WRL 68 cells; Neurosphere; C2C12 cells; Bioscaffold*

Introduction

Cell culture offers the consistency and reproducibility of results and for that reason it is used as a valuable tool in biological research. It became a common approach for the investigation of morphological, biochemical and physiological properties of cells as well as large scale manufacturing of biological compounds. Conditions that allow growing cells in vitro vary according to a type of the cells (5). They create the artificial environment in which the cells are maintained in a suitable dish containing a culture medium. Some cell types can be grown floating in suspension culture while the others require attachment to a solid or semisolid substrate. When cells with migratory and proliferative potential are cultured in vitro on an adhesive surface they grow in a sheath to form a monolayer. This anchorage-dependent approach to cell cultivation allowed studying biology of individual cells, to establish continuous cell lines, which laid down the basis for modern cellular and molecular biology. However, traditional two-dimensional (2D) systems have a number of drawbacks. Most importantly they do not reflect closely the conditions under which the cells interact in living tissues. Behaviour of cells grown in planar systems differs from those observed in vivo. The cells cannot maintain correct morphology and adopt flattened shapes (26).

Retention of histological structure and organotypic function is possible when the cells are grown in three-dimensional (3D) culture systems (4, 13). Cells grown in 3D contexts closely resemble in vivo situation as they respond to the geometry of their environment and also display excellent functional characteristics. There are two major approaches to 3D cultivation (6). The first is based on explantation of whole fragments of tissue that are maintained in an organ culture. The second recombines the cell lineages using histotypic or organotypic cultures. 3D systems are suitable for the developmental studies, screening and drug discovery procedures, modelling disorders including malignant invasion in vitro and testing new therapies. Last but not least, the need for 3D culture systems is crucial for tissue engineering and preparation of new tissue constructs.

In this study we describe and compare morphological analyses of three different approaches for generation of histotypic cultures: multilayered cultures of WRL 68 hepatocytes grown on semipermeable membranes, spheroids generated by neural stem/progenitor cells called neurospheres, and acellular muscle scaffolds recellularized with C2C12 myoblasts.

Material and Methods

Cultivation of WRL 68 cells

WRL 68 cell line (ATCC, USA) of human fetal hepatocytes was cultured in EMEM medium (BioWhittaker, Cambrex,

USA) supplemented with 10% fetal bovine serum (FBS; Gibco, Invitrogen USA), glutamine, penicillin 100 U/ml and streptomycin 100 µg/ml (Sigma-Aldrich, Czech Republic) at 37 °C in a humid atmosphere of 95% air and 5% carbon dioxide. WRL 68 cells were grown in a monolayer or 3D cultures. A monolayer was obtained by growing the cells in culture flasks (Nunc, Denmark) and passaging them twice per week (split ratio 1 : 15). Cells in a monolayer were grown for 9 days only. For a long-term (12 weeks) and 3D growth in vitro, 250,000 cells were cultured on a special 25-µm thick plastic bottom membrane in PetriPerm dishes (Vivascience, Germany) that is well permeable to oxygen and carbon dioxide. The culture medium was changed three times a week.

The viability test was performed with propidium iodide 50 µg/ml added to the culture for 10 min after a thorough washing of cells with PBS under TE 300 Eclipse (Nikon, Japan) equipped with epifluorescence.

Neurosphere assay

Suspension of cells isolated from the developing rat brain on embryonic day 14 was obtained after trypsinization and gentle mechanical trituration using a micropipette in glucose-saline solution containing DNase I. The neural cells were plated at a density 15,000 cells/µl in a chemically-defined serum-free medium composed of a 1:1 mixture of DMEM (Gibco) and Ham's F12 nutrient containing N2 (Gibco) and B27 supplement (Life Technologies, MA, USA) with 10 ng/ml bFGF and 20 ng/ml EGF (PeproTech, UK). Cultures were maintained in medium at 37 °C in humidified atmosphere consisting of 95% air and 5% carbon dioxide. Half the volume of the medium was replaced twice a week with a fresh medium.

Cultivation of C2C12 cells

C2C12 mouse adherent myoblasts (Sigma-Aldrich) were grown in Dulbecco's modified Eagle's medium (DMEM) supplemented with heat-inactivated 10% fetal bovine serum, 2 mM glutamine, penicillin 100 U/ml and streptomycin 100 µg/ml (Sigma-Aldrich), pH 7.5. After reaching 80% confluency after 2–3 days in vitro the cells were passaged. The cell line was maintained in a 5% CO_2 atmosphere at 37 °C and cell viability was assessed by the Trypan Blue (Life Technologies, MA, USA) exclusion test. For scaffold recellularization, 2 to 3 acellular scaffolds were placed in 6 well plates dishes and these were exposed to 10^5 cells per ml of cultivation medium. Cultivation medium was replaced with fresh solution every three days.

Preparation of decellularized muscle scaffolds

All procedures were approved by the Ethical Committee supervising procedures on experimental animals at Charles University Medical Faculty in Hradec Králové. Tibialis anterior (TA) muscle was isolated from sacrificed C57Bl/6J mice and cut in pieces 3 × 6 mm. After washing with PBS buffer, muscle pieces were incubated in sterile 5M NaCl in distilled water for 2 h at 4 °C under slow agitation and then immersed into hypotonic 10 mM TrisHCl for 22 h at 4 °C under slow agitation. The next step included incubation with 1% SDS in distilled water for 24 h at room temperature under slow agitation. Scaffold was sterilized by 0.1% peracetic acid solution titrated to pH 7.0 for 4 h at room temperature under slow agitation. PBS buffer applied for 24 h at 4 °C assured washing out cell residues. DNA content in scaffolds was decreased with DNase (Promega, WI, USA) applied for 1 h at 37 °C followed by washing with fresh PBS buffer.

Histology

3D cell formations yielded from cultures were processed for histology to assess the cell morphology and ratio of cell differentiation. The samples were immersed in neutral buffered formalin for 30 min at room temperature. The scaffolds were fixed by 4% paraformaldehyde (Sigma-Aldrich) overnight. Following dehydration with increasing concentrations of ethanol and exposure to xylene, the samples were embedded in melted paraffin. After cooling the tissue blocks were cut to 7-µm thick sections using sliding microtome Leica SM2000R. The sections were attached to the slide with alum gelatine and after deparaffinization and rehydration they were stained with hematoxylin and eosin, Masson's green trichrome or processed for immunocytochemistry.

Alternatively the samples were fixed in mixture of 1% paraformaldehyde and 1% glutaraldehyde (Sigma-Aldrich) for 4 hours and following a thorough washing with phosphate buffer they were fixed with 2% osmium tetroxide (SPI Supplies, PA, USA) for 90 min and immersed in 2% uranyl acetate (Sigma-Aldrich) for 30 min. After washing with sodium acetate and 10% saccharose, the tissue was dehydrated with increasing concentrations of ethanol, transferred to propylene oxide (Sigma-Aldrich) and embedded in Durcupan-Epon resin (Sigma-Aldrich). The tissue blocks polymerized at 60 °C for 60 hours and then the semithin sections were cut on Ultrotome Nova (LKB, Sweden) and stained with toluidine blue.

Immunocytochemistry

Sections of WRL 68 cells were incubated for 20 min in methanol containing 1% H_2O_2 to reduce endogenous peroxidase activity. For antigen retrieval, the sections were exposed to microwaves (700 W) in sodium citrate solution for 2 × 5 min. After thorough washing in 0.2M Tris-HCl buffer containing 0.5% Triton X-100 (Sigma-Aldrich), the sections were exposed to primary antibodies against M30 neoepitope (Roche Life Science, IN, USA) for 45 min. After washing, sections were incubated with anti-mouse secondary biotinylated antibody (Sigma-Aldrich) for 45 min and then with streptavidin labelled with horseradish peroxidase

(BioGenex, CA, USA). After rinsing, the reaction was developed using DAB (3,3′-diaminobenzidine tetrahydrochloride, Sigma-Aldrich) and H_2O_2. Sections were then counterstained with methyl green, dehydrated and mounted in DPX mounting medium (Sigma-Aldrich).

Results

3D cultures of WRL 68 cells

WRL 68 cells proliferated briskly and in 3–4 days in vitro they reached 70% confluence (Fig. 1A). Propidium iodide labelled only a minor fraction of cells (0.95–1.48%). Without passaging the cells reached 100% confluence within a week and started to grow over each other. However, basal cells overgrown by new overlaying cell layers suffered with deficit in oxygen, changed their morphology and started to degenerate and ultimately die.

Cultivation in PetriPERM dishes avoided the initial cell degeneration due to cell hypoxia and allowed the cell stratification. In the second week the areas containing several cell layers were separated by areas covered by a cell monolayer. An intense growth is reflected by the finding of mitotic cells inside of the multilayered structure (Fig. 1B and 1C). After 3 weeks in vitro, the whole bottom of the PetriPERM dishes was covered by several cell layers; the thickness of a cell layer varied from 2 to 8 cells. Histological examination revealed the basal cells assumed a flattened morphology, inner lying cells were polygonal whereas the upermost cells had spherical or oval shapes. Almost all the cells were in contacts with cell membranes of other WRL 68 cells. The cells contained one to two cell nuclei and pale but basophilic cytoplasm. Rarely cells undergoing cell death were encountered. The eosinophilic cytoplasm of apoptotic cells surrounded pycnotic nucleus; some nuclei were fragmented. After a complete decay of few adjacent cells small empty spaces were left between the viable cells; rarely apoptotic bodies were encountered inside of these spaces. After a 6-week cultivation the cells accumulated in 8–9 layers. However, the number of viable cells decreased and as a result only some cells were in a complete contact with their neighbours. The cells of a basal layer remained viable even in a long-term culture. Other viable cells were found as single cells not forming intercellular junctions. They had a large cell nucleus and pale basophilic cytoplasm. The number of cells with the eosinophilic cytoplasm increased. The cellular mass contained the cells reflecting different features of programmed cell death: condensed chromatin, karyorrhexis and apoptotic bodies. Eosinophilic cells expressed M30 neoepitope confirming that cells were dying by apoptosis (Fig. 1D). Intensity of an immunoreactive signal varied; some cells were stained weakly while the others (especially small cells and apoptotic bodies) expressed a strong signal in their cytoplasm. M30-positive cells were of different sizes and bizzare shapes whereas negative cells were oval or polyedric. Histological examination of sections through the PetriPERM membrane covered with layers of WRL cells harvested from culture after 12 weeks identified eosinophilic cellular mass consisting of degenerating cells. There were only few viable cells often connected together. Nevertheless, a basal layer of flattened cells remained well preserved.

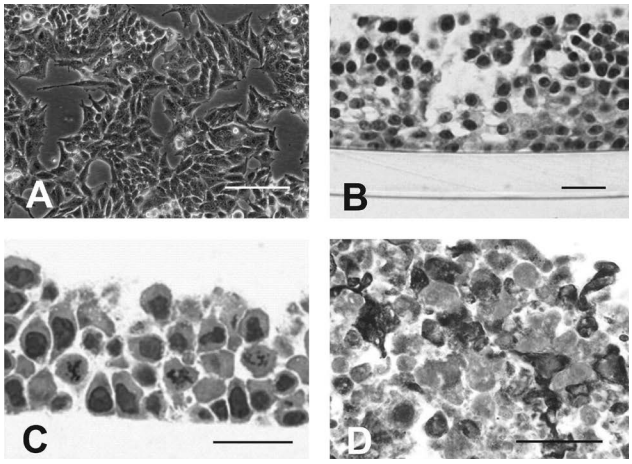

Fig. 1: Culture of WRL 68 cells. A) Phase contrast of a WRL 68 cell monolayer 3 days after seeding showed the subconfluent cells with a uniform morphology. Rounded cells corresponded to dividing and dying cells as both events involved retraction of cytoplasmic processes and detachment from junctions with adjacent cells. B) After a 9-day cultivation in a PetriPerm dish (visible at bottom) WRL 68 cells grew over the others in several layers. Small cavities and empty spaces appeared among the cells but the basal layer remained always continuous. C) A detailed view of a short-term (9-day) culture with cells arranged in 5 layers. The cells were mononucleated, uniform in morphology and size and connected via intercellular junctions; few cells underwent mitotic division. D) Immunohistochemical detection of M30 neoepitope gave evidence of frequent apoptosis in cells harvested from a long-term (12-week) culture. The positive cells had bizzare shapes; the signal was absent from the cell nucleus, which often shrinked. The dying cells were localized between intact cells in all cell layers of a 3D culture. Scale bar 50 μm in A, 25 μm in B–D.

3D cultures of neural progenitor cells

In serum-free cultivation media differentiated neural cells rapidly died and only neural progenitor and stem cells survived and responded to stimulation with growth factors by repetitive cellular divisions. The newly generated cells remained adhered together, which resulted in formation of multicellular floating spheroids, called neurospheres. Under ideal conditions, each neurosphere represented a clone of a single founder cell, however, at high cell densities, some cells could adhere and small neurospheres were also fusing together forming larger spheroids within few days. The edge of neurospheres had sharp and smooth contours (Fig. 2A). Without passaging the neurospheres increased their sizes rapidly in the course of the first two weeks in vitro. At the end of the first week many neurospheres reached sizes over 50 μm.

Histological examination revealed that densely packed small cells occupied the superficial 2–4 layers (Fig. 2B). The peripheral cells were basophilic and some underwent mitotic division. A cellular density in a central region of larger neurospheres was lower when compared with peripheral areas. Rarely fragments of pycnotic chromatin were also noticed demonstrating that cell death also occurred in early neurospheres. Semithin sections of neurospheres harvested in the second and third week of cultivation showed similar results. The cells started to differentiate and as a result the cell population was heterogeneous. Superficial cells were more immature than cells lying in the central region: they were smaller and densely arranged. Mitotic figures were not frequent but if they appeared they were localized to the layers of superficial cells. All nuclei of cells occupying the central core were in the interphase and they often contained the nucleolus. Bodies of these cells were larger and paler and sent elongated cytoplasmic processes. Apoptotic cells or apoptotic bodies observed between the groups of viable cells were more frequent than dividing cells (Fig. 3C). These cells were small, contained fragments of condensed chromatin and represented 3–5% of all cells. Small cavities that had sizes of cells were distributed over the neurosphere and sometimes contained a shrinked dying cell. After one and two months of cultivation in a dish the neurospheres were still viable, they grew larger and showed similar microscopic features. A central region contained cells that showed regular signs of cell regression with eosinophilic cytoplasm and shrinked chromatin (Fig. 2D). A peripheral region still contained viable and intact cells. Differentiated cells were localized to deeper layers whereas less mature cells occupied outermost layers. If the neurosphere attached to a bottom of a culture dish, the neurosphere basis contained less cells than the free edges.

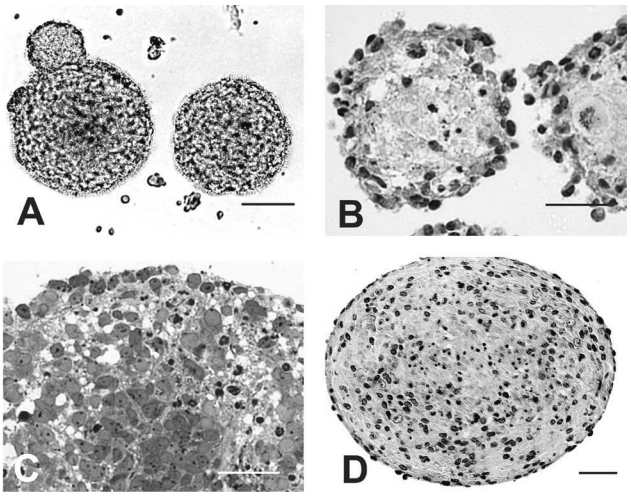

Fig. 2: Culture of neurospheres. A) Phase contrast of nerospheres after 5 days in vitro showed their regular shapes and outlines. The left neurosphere fused with smaller one. B) Semithin sections revealed the inner structure of the early neurospheres: The periphery was occupied by small basophilic cells arranged in few layers; mitotic divisions were confined to this zone. Central areas were less cellular and contained cells with pycnotic and fragmented chromatin. C) In 9-day neurospheres, programmed cell death was relatively common. Cells with pycnotic and fragmented nuclei were usually seen in areas with small empty spaces. Central areas accumulated lots of differentiating cells with cytoplasmic processes. Intact cells in the interphase overnumbered the dying cells. D) In long-term cultures, dying cells were distributed in central less cellular areas. A paraffin-embedded section of an 8-week neurosphere showed intact and differentiated cells in a peripheral belt. Scale bar 50 μm in A, B, D, 25 μm in C.

3D scaffolds colonized with C2C12 cells

C2C12 cells plated in dishes first had typical starshaped or fusiform morphology. Only dividing cells were rounded. As mononucleated cells became closely adherent they elongated. After four days, first cells started to fuse. The cell fusion gave rise to multinucleated structures that grew larg-

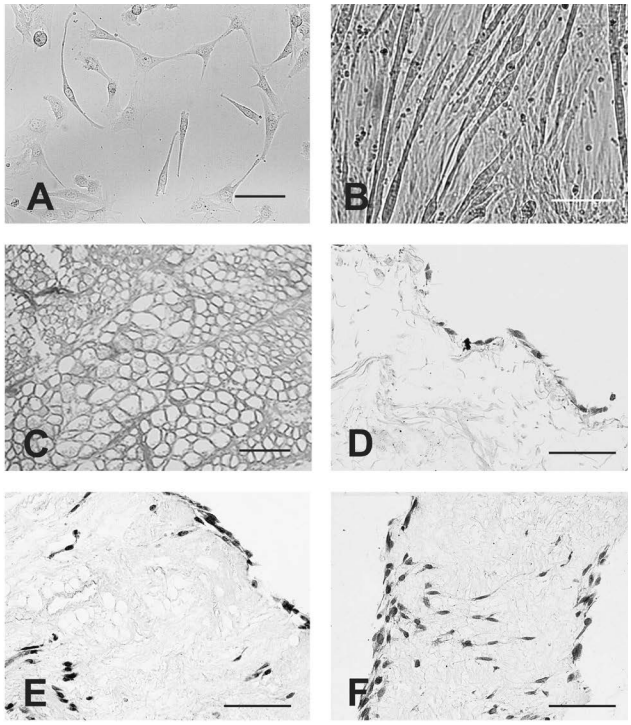

Fig. 3: Culture of C2C12 cells and scaffolds. A) Phase contrast of C2C12 cells 2 days from passaging showed a spindle shaped to flatten morphology of mononucleated myoblasts. B) Cultivation in 10% of horse serum resulted in cell fusion and appearance of elongated myotubes containing multiple nuclei. C) Histology of an acellular muscle scaffold confirmed absence of myofibres and cell nuclei. Extracellular matrix was well preserved and reflected a basic structural plan of the skeletal muscle. D-F) Scaffolds recellularized with C2C12 cells 3- (D), 6- (E), and 9-day (F) cultivation were covered with viable cells that started to penetrate inside. Most cells were mononucleated although a close cell apposition was observable on day 9. Scale bar 25 μm in A, 50 μm B, 100 in C and 150 μm in D–E.

er reaching the length of several hundred micrometers. In confluent cultures these myotubes appeared regularly. For colonization of acellular scaffolds undifferentiated mononucleated myoblasts were used. The scaffolds devoid of cells were cut to small pieces with the length not exceeding 3 mm and diameter below 2 mm before they were exposed to C2C12 cells. Decellularized scaffolds were processed for histology as a control prior seeding with cells. Masson's Green trichrome staining gave evidence that extracellular matrix, namely collagen fibres and bundles, was well preserved and organized in a muscle tissue-specific manner. Empty spaces left after a removal of muscle fibre cytoplasm showed parallel arrangement and were delineated with the thin endomysium. The perimysium, epimysium and tendons contained more abundant extracellular matrix. Lumina of sporadic medium-sized blood vessels running through the tissue were observable but they lacked a simple squamous endothelial lining. Histological examination verified the absence of any cells and muscle fibres; fluorescence was used to confirm that no cell nuclei were left in decellularized scaffolds. Re-seeding of scaffolds with C2C12 cells confirmed the murine myoblasts well adhered to its extracellular matrix and they remained viable. Cell morphology and cell migration along the scaffolds was examined in paraffin-embedded sections at 3, 6 and 9 days after cultivation. Three days in vitro the cells migrating over the outer surface adopted bipolar and flattened morphology. The cells had basophilic cytoplasm and extended thin cytoplasmic processes. They were mostly arranged in a single discontinuous layer; cells overlapping did not occur. Three days later, on day 6 of their in vitro cultivation, C2C12 cells attaching to the outermost surfaces increased in cell numbers and formed one to three continuous layers. Some cells entered inside of the scaffolds and migrated through the extracellular matrix as single cells. The cells were elongated with basophilic cytoplasm and single nucleus. Inside the scaffold the cells formed small groups usually on top surfaces of collagen bundles. By day 9 in vitro more cells accumulated in some deep areas of scaffolds while the other places were left unoccupied which likely reflected a varying accessibility. The myogenic cells entering inside represented less than 10 % of all cells that remained in a contact with the scaffold. Interior cells were arranged in the same orientation in space as they occupied tubular spaces left after removal of original skeletal muscle fibres. Few cells that came to a close contact started to fuse but the number of multipotent cells was still very small. Majority of cells that covered the outer surface or recellularized interior of scaffolds were of bipolar to fusiform shapes and mononucleated. No myotubes, polyploidy giant cells or dying cells were detectable in short-term cultures of recellularized scaffolds.

Discussion

Cells of multicellular organisms are in mutual contacts with the neighbouring cells and components of extracellular matrix that are arranged in all directions. The cells can be isolated from the tissues and grown in vitro to study their complex biological functions. Most current approaches prefer cell cultivation as a monolayer due to simplicity although it does not reflect the whole tissue complexity. Nevertheless 2D systems allowed optimization of basic culture conditions including composition of cultivation medium and its supplementation with growth factors.

3D cell cultivation requires different approaches. There are few general requirements such as sufficient cell viability, growth, adherence, differentiation potential and stability. This study described data for 3D cultures prepared by stratification of cells grown on a semipermeable membrane, forming spheroids in a non-adherent system and supporting cell migration along the z-axis with a suitable scaffold.

We utilized WRL 68 cells for cultivation of hepatic cells as the WRL 68 cells can be split in new culture dishes with the ratio 1 : 20 after passing. Adult liver cells exhibit low growth potential and cannot be maintained in culture for long time limiting their study to few days in vitro. A primary culture of embryonic hepatocytes can be grown for few weeks due to initially large proliferative capacity; however, they cannot be passaged successfully. A high mitotic activity of WRL 68 cells allows cell overlapping and stratification, which is a feature of complex epithelia. Diffusion of oxygen and nutrients is a limiting factor counterbalancing number of cell layers and thickness of the entire multicellular formation. With an increasing size the centrally lying cells are not well nourished and undergo regression. Apoptotic WRL 68 cells expressed M30 neoepitope formed by cleavage of cytokeratin 18 (Fig. 1D). Cultivation of cells attached to semipermeable dishes supplied the 3D cell formations with oxygen allowing them to reach larger sizes. But in the long-term culture frequent cells enter cell death. Although the WRL 68 cells grown in a long-term 3D culture increase expression of the membranous transporters Mdr1 and Mrp2 (3) they do not reflect pattern of polarized hepatocytes. One prerequisite for cell polarization is making contacts with variety of multiple cell types that participate in tissue construction to form its stroma, nerves and blood or lymphatic vessels. Co-culture of different cell types could yield better results. For example the hepatocyte–sinusoid alignment supports liver regeneration (8).

Although primary embryonic neural cells can spontaneously cluster and migrate along axons and radial glia fibers (12) they do not grow in multiple layers. On the contrary when multicellular cell clusters are put on a cultivation dish, the neural cells prefer to emigrate and spread in a monolayer. While nervous cells are postmitotic, neural progenitor and stem cells represent an ideal source that can generate any neural cells. The neurosphere assay established by Reynolds and Weiss (23) was used to maintain the cells in the undifferentiated phenotype in case the neurospheres are passaged regularly. Cell differentiation is prevented by regular cell dissociation while the resulting cells are not allowed to anchor to a substrate. Mitogenic effects of epidermal and fibroblast growth factors drive proliferation of progenitor

and stem cells. When grown in small cell densities, each neurosphere arises as a cell clone. The size of neurosphere derived from neural progenitor is different from those derived from stem cells (24). Simultaneous growth factor stimulation leads to symmetric divisions of undifferentiated cells inside of neurospheres and to cell expansion. In the growing neurosphere, the resulting cell number is balanced by cell proliferation and cell death. The cells in the neurosphere grown without passaging undergo spontaneous cell differentiation that reflects characteristic zonal arrangement: immature cells incl. progenitors occupy the peripheral belt whereas neurons and astroglia are localized in the central core. Cells of the long-term neurospheres can reach their terminal differentiation. Oligodendrocytes are able to cover the axons with myelin sheaths and neurons make interneuronal synapses containing synaptic vesicles. Astrocytes can form perivascular limiting membrane as demonstrated by intracerebral transplantation of solid neurospheres (14, 15). Similar microscopic structure and basic cell arrangement can be expected in other spheroids grown in vitro including cardiospheres and mammospheres (1, 2).

Another strategy how to prepare 3D culture from the cells that do not stratify or form spheroids is to provide them a support in a form of 3D latticework using suitable gels or scaffolds. Matrigel consists of a mixture of gelatinous glycoproteins (e.g., laminin, collagen, entactin etc.) enriched for bioactive molecules (e.g., growh factors, metalloproteinases) isolated from mouse sarcoma. In cell cultures Matrigel was used to navigate the endothelial cells to form 3D tubes mimicking the blood vessels (21) or to grow the primitive alveoli by epithelial cells of the mammary gland (17). A good example of artificial gels is a hydrogel based upon polyethyleneglycol and fibrinogen that promotes muscle fibre formation after short-term cultivation with mesoangioblasts (7).

Biogenic scaffolds are superior to fabricated artificial materials. Tissue decellularization (9) offers an alternative to obtain scaffolds formed by the extracellular matrix that reflect tissue microstructure and contain bioactive molecules supporting cell attachment and organisation. Moreover, acellular tissue scaffoldings offer several potential advantages as they are immunologically inert, retain extracellular proteins, basal laminas, and stromal components that facilitate cell incorporation in vivo. Moreover, they contain remnants of the acellular native vascular network that allow to perfuse the construct. Our short-term in vitro study of cell colonization of scaffolds obtained from a decellularized skeletal muscle demonstrates their good biocompatibility. C2C12 cells that adhere and migrate over the surfaces eventually enter the scaffold interior to be organized in three dimensions. The immigrating cells are not arranged randomly; instead they are organized along the inner parallel tube-like spaces. The cell density of recellularized scaffolds does not correspond to density of neurospheres or tightly stratified layers of WRL 68 cells grown in PetriPerm dishes but this obstacle could be solved by pretreatment with chemoattractant and growth factors or by a careful selection of cells used for recellularization. On the other hand, the cells inside the muscle scaffolds remain viable, do not show any abnormal changes, any signs of regression or cell death, which speaks in favour of biogenic scaffolds derived from the tissue extracellular matrix. Recently several groups established a proof of concept for utilization of decellularized bioscaffold reseeded with cells in reengineering of complex bioartificial organs like the heart (19), lung (20) or liver (25). Such organs are transplantable and functional as demonstrated by Uygun et al. 2010 in liver grafts (25) or by Olausson et al. 2012 in veins (18).

Conslusion

There exist many more alternatives to methods that permit the researchers to grow the cells in 3D culture systems, especially the cells with a low proliferative and migration capacity. Some are based on forced or passive cell aggregation examples of which include culturing the cells in rotating bioreactors or hanging drops used to produce embryoid bodies. Rotating bioreactors facilitating diffusion of cultivation medium are useful in short-term organotypic cultures (4, 13). Cell 3D printing became a novel sophisticated tool that allows precise positioning of cells in space in combination with selection of suitable biomolecules to create optimal microenvironment that mimics microarchitecture of native tissues (16). Combination of 3D culturing with a promising potential of pluripotent stem cells opens a new avenue for generation of organoids or miniature organs. Recent reports announced a successful construction of several mini-organs including renal, intestinal and cerebral organoids (11, 27, 28).

3D cell constructs generated in vitro mimic embryonic development, closely resemble tissue morphology and also display excellent functional characteristics, which determine these powerful systems to model organogenesis, disease pathogenesis, screen drugs, test new therapies and even to construct replacement tissues.

Acknowledgements

This work was supported by the European Social Fund, the state budget of the Czech Republic Project No. CZ.1.07/2.3.00/30.0061, Prvouk P37/06 and SVV-2015-260179.

References

1. Beltrami AP et al. Adult cardiac stem cells are multipotent and support myocardium regeneration. Cell 2003; 114: 763–76.
2. Cioce M et al. Mammosphere-forming cells from breast cancer cell lines as a tool for the identification of CSC-like- and early progenitor-targeting drugs, Cell Cycle 2010; 9: 2950–9.
3. Cizkova D, Mokry J, Micuda S, Osterreicher J, Martinkova J. Expression of MRP2 and MDR1 transporters and other hepatic markers in rat and human liver and in WRL 68 cell line. Physiol Res 2005; 54: 419–28.

4. Freed LE, Vunjak-Novakovic G. Tissue culture bioreactors: Chondrogenesis as a model system. In: Lanza RP, Langer R, Chick WL eds. Principles of tissue engineering. Austin, USA: Academic Press, 1997: 151–65.
5. Freshney RI. Culture of specific cell types. In: Culture of animal cells: A manual of basic technique (2nd ed.). New York: Alan R. Liss Inc., 1988: 257–80.
6. Freshney RI. Three-dimensional culture systems. In: Culture of animal cells: A manual of basic technique (2nd ed.). New York: Alan R. Liss Inc., 1988: 297–307.
7. Fuoco C et al. In vivo generation of a mature and functional artificial skeletal muscle. EMBO Mol Med 2015; 7: 411–22.
8. Hoehme S et al. Prediction and validation of cell alignment along microvessels as order principle to restore tissue architecture in liver regeneration. Proc Natl Acad Sci USA 2010; 107: 10371–6.
9. Hrebikova H, Diaz D, Mokry J. Chemical decellularization: A promising approach for preparation of extracellular matrix. Biomed Pap 2015; 159: 12–7.
10. Laerum OD, Bjerkvig R. Monolayer and three-dimensional culture of rat and human central nervous system: Normal and malignant cells and their interactions. Meth Neurosci 1990; 2: 210–36.
11. Lancaster MA, Knoblich JA. Generation of cerebral organoids from human pluripotent stem cells. Nat Protoc 2014; 9: 2329–40.
12. Liour SS, Yu RK. Differentiation of radial glia-like cells from embryonic stem cells. Glia 2003; 42: 109–17.
13. Mazzoleni G, Di Lorenzo D, Steimberg N. Modelling tissues in 3D: The next future of pharmaco-toxicology and food research? Genes Nutrition 2009; 4: 13–22.
14. Mokry J, Karbanova J, Filip S. Differentiation potential of murine neural stem cells in vitro and after transplantation. Transplant Proc 2005; 37: 268–72.
15. Mokry J, Subrtova D, Nemecek S. Differentiation of epidermal growth factor-responsive neural precursor cells within neurospheres. Acta Med 1996; 39: 7–20.
16. Murphy SV, Atala A. 3D bioprinting of tissues and organs. Nature Biotechnol 2014; 32: 773–85.
17. Murtagh J, McArdle E, Gilligan E, Thornton L, Furlong F, Martin F. Organization of mammary epithelial cells into 3D acinar structures requires glucocorticoid and JNK signaling. J Cell Biol 2004; 166: 133–43.
18. Olausson M et al. Transplantation of an allogeneic vein bioengineered with autologous stem cells: A proof-of-concept study. Methods Mol Biol 2012; 798: 21–52.
19. Ott HC et al. Perfusion-decellularized matrix: Using nature's platform to engineer a bioartificial heart. Nat Med 2008; 14: 213–21.
20. Petersen TH et al. Tissue-engineered lungs for in vivo implantation. Science 2010; 329: 538–41.
21. Ponce ML. Tube formation: an in vitro matrigel angiogenesis assay. Methods Mol Biol 2009; 467: 183–8.
22. Qing Q, Qin T. Optimal method for rat skeletal muscle decellularization. Chin J Rep Rec Surg 2009; 23: 836–9.
23. Reynolds BA, Weiss S. Generation of neurons and astrocytes from isolated cells of the adult mammalian central nervous system. Science 1992; 255: 1707–10.
24. Reynolds B, Rietze RL. Neural stem cells and neurospheres – re-evaluating the relationship. Nature Methods 2005; 2: 333–6.
25. Uygun BE et al. Organ reengineering through development of a transplantable recellularized liver graft using decellularized liver matrix. Nat Med 2010; 16: 814–20.
26. von der Mark K, Gauss V, von der Mark H, Müller P. Relationship between cell shape and type of collagen synthesised as chondrocytes lose their cartilage phenotype in culture. Nature 1977; 267: 531–2.
27. Watson CL et al. An in vivo model of human small intestine using pluripotent stem cells. Nature Medicine 2014; 20: 1310–4.
28. Xia Y et al. Directed differentiation of human pluripotent cells to ureteric bud kidney progenitor-like cells. Nat Cell Biol 2013; 15: 1507–15.

Received: 16/06/2015
Accepted in revised form: 09/09/2015

Corresponding author:

Prof. MUDr. Jaroslav Mokrý, Ph.D., Charles University in Prague, Faculty of Medicine in Hradec Králové, Šimkova 870, 500 38 Hradec Králové, Czech Republic; e-mail: mokry@lfhk.cuni.cz

ORIGINAL ARTICLE

DEEP NECK INFECTIONS OF ODONTOGENIC ORIGIN AND THEIR CLINICAL SIGNIFICANCE. A RETROSPECTIVE STUDY FROM HRADEC KRÁLOVÉ, CZECH REPUBLIC

***Helena Doležalová*[1], *Josef Zemek*[2], *Luboš Tuček*[1]**

Department of Dentistry, Faculty of Medicine, Charles University, and University Hospital in Hradec Králové, Czech Republic[1]; Department of Computer Systems, University Hospital in Hradec Králové, Czech Republic[2]

Summary: Introduction: Cellulitis remains a very serious disease even today. Mortality, which varied between 10–40%, has been reduced owing to the standard securing of airway patency and use of an appropriate surgical treatment approach.
Materials and methods: A total of 195 patients were hospitalised for cellulitis at the University Hospital in Hradec Králové during 2007–2011. The following parameters were evaluated: age, gender, dependence of incidence of the disease on the season of the year, frequency of attacks of the particular areas and their clinical characteristics, aetiology of the inflammation, types of patient complaints, prevalence of current systemic diseases, results of microbiological and selected laboratory analyses, socio-economic status of the patients, and duration of patient stay at the hospital. Statistical analysis was performed by using Pearson's correlation coefficient, the statistical significance level was $p < 0.05$.
Results: The mean age of the patients was 39.8 years. The group of 195 patients included 108 (55%) males and 87 (45%) females. The mean time between the first symptoms of the disease and admission to the Department was 5 days. From among the 195 patients, 116 (59.5%) were working persons, 79 (40.5%) were non-working (children, students, unemployed persons, women on maternity leave, retired people). The odontogenic origin of the disease was verified in 173 (88.7%) patients. In total, 65 (33.3%) patients had no coinciding complicating systemic disease, 22 (11.3%) patients had diabetes mellitus. The most frequent symptom of cellulitis was painful swelling, found in 194 (99.5%) patients, followed by jaw contracture, found in 153 (78.5%) patients.
Conclusion: The results are largely very similar to those of previous studies performed in other countries, except that we found no correlation between the prevalence of cellulitis and the socio-economic status, nor have we confirmed *Klebsiella pneumoniae* sp. as the cause of cellulitis in patients with diabetes mellitus.

Keywords: *Cellulitis; Odontogenic infection; Oral microflora; Bacteria*

Introduction

Even today, inflammatory processes in maxillo-facial areas – cellulitis, or deep neck inflammations, are regarded as very serious diseases that can threaten patient's health and life. Such inflammations can be categorised aetiologically into inflammations of odontogenic origin and inflammations of non-odontogenic origin. The former predominate (70–90%) in adult patients, whereas the latter predominate in paediatric patients.

Cellulitis is largely caused by mixed aerobic/anaerobic bacterial microflora, which routinely colonises the oral cavity and does not primarily consist of pathogenic microbial species. Clinically, cellulitis includes mostly suppurative inflammation, with the tendency to delimiting and formation of abscesses. However, cellulitis can also develop into a formation of phlegmonous nature and can then propagate rather readily into anatomically quite remote preformed areas in the head and neck area. Older published data postulated that the incidence, severity, morbidity and mortality of cellulitis have decreased significantly during the past decades (1). This information is in direct contradiction to our current clinical experience. The amount of cellulitis is increasing with more severe clinical course. Among the factors that contributed to this success were early diagnosis, introduction of radical surgical treatment and use of modern, highly efficacious antibiotics. Despite this major advance in the treatment of cellulitis, we must be prepared at any moment to face an unexpected situation and/or complications that can accompany cellulitis therapy (including enhanced bacterial resistance and the associated insensitivity of a number of bacterial agents to various antibiotics). Once appeared, cellulitis complications are a constant cause of very high (50%) mortality (2).

When assessing the severity and prognosis of cellulitis, attention must be paid, in particular, to warning signs indicating propagation of infection through the body, such as body temperature increase above 39 °C, appreciable

ACTA MEDICA (Hradec Králové) 2015; 58(3): 86–91
http://dx.doi.org/10.14712/18059694.2015.98

jaw contracture, signs of inflammation spreading to the surroundings along the large neck vessels, oedema or skin reddening in the jugular area, pain under the sternum, but also swollen eyelids and retrobulbar pain, stridor, cough and pain in the chest (3–5, 1). Appropriate timing of surgical intervention is an important factor in cellulitis therapy: it should be conducted early and correctly, adhering (also today) to the rule "*Ubi pus, ibi evacuo…*"

No recent information on the situation in the incidence, severity, cause(s) and occurrence of complications in cellulitis of odontogenic origin in the Czech Republic is available except for one paper focusing on the issue of severe complications accompanying deep neck inflammations (6). Therefore the authors of the present paper performed analysis of this severe disease in a group of patients treated during the 5-year period of 2007–2011 at the authors' workplace, i.e. the Maxillo-facial Surgery Unit, Department of Dentistry, Faculty of Medicine, Charles University, and Teaching Hospital in Hradec Králové, Czech Republic, where the majority of patients with this disease from the East Bohemian region have been treated. The authors of this contribution also compared their own findings with those recently published by other authors.

Material and methods

The study was approved by local ethical commitee. A total of 195 inpatients with the diagnosis of cellulitis were treated at the Maxillo-facial Surgery Unit, Department of Dentistry, Faculty of Medicine, Charles University, and Teaching Hospital in Hradec Králové, during 2007–2011. Outpatients with similar diagnoses were not included in the study. All the patients were examined by the adequate routine procedure, and where their health permitted so, subjected to panoramic X-raying and ultrasound examination. The results were entered into the patient's medical records and the patient was then referred to the maxillo-facial surgery unit for admission. The patient's medical history record was then compiled, including the diagnosis with which the patient had been referred, the name of the referring physician, length of the disease from the first symptoms to the date of admission, any previous medical treatment and its effect, past tooth extractions, final diagnosis of some form of cellulitis and the treatment plan. Prior to the surgery, performed in general anaesthesia, the patients were subjected to routine preoperative assessment, including examination at the anaesthesiology centre. The centre decided if and how the patient can be intubated. Many patients were intubated by the flexible fibroscopic method. Therefore they were transferred to the inpatient ward of the Department of Anaesthesiology, Resuscitation, and Intensive Medicine (KARIM), where they were extubated later, usually during the next 48 hours. In some clear cases where abscess centres were present without previous radiographic examination.We performed external incision and drainage under local anaesthesia. All patients in whom intraoral mucous membrane incision was feasible were treated in local anaesthesia. Pearson's correlation coefficient was used for statistical evaluation of the parameters. Statistical analysis between elevated body temperature and the CRP level, body temperature and the leukocyte count, leukocyte count and the CRP level, duration of the cellulitis treatment and the leukocyte, duration of the treatment on the CRP level. The statistical significance level was $p < 0.05$.

Results

The group of patients included in this study comprised 108 (55%) males and 87 (45%) females (Graph 1). The number of cellulitis inpatients was highest in February (25 patients) and in June (24 patients) and lowest in November (5 patients) (Graph 1). The number of inpatients treated during a defined time period was steady during the years included, only in 2009 it was appreciably lower. The mean patient age and the median were 39.8 years and 36 years, respectively. The youngest patient was aged 4, the oldest patient 91. The group included 116 employed and 17 un-

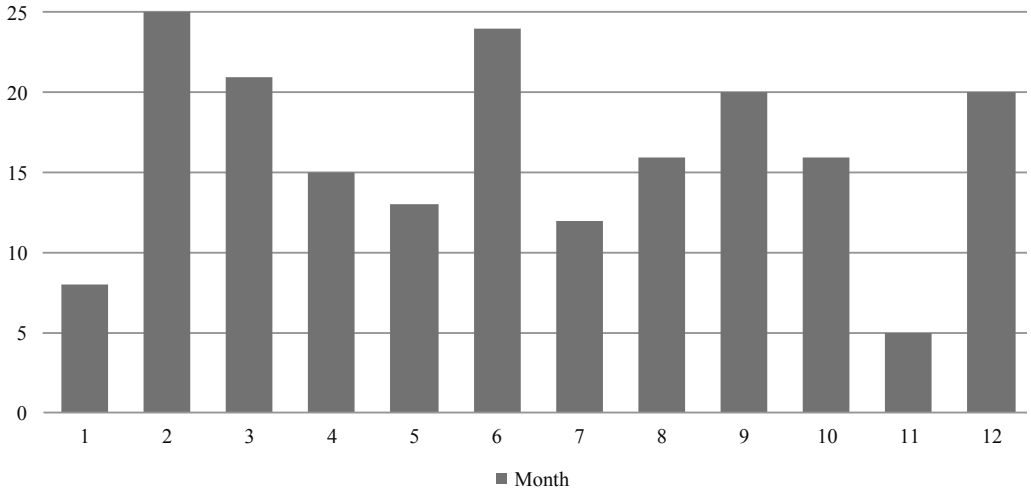

Graph 1: Distribution of the patients throughout the year seasons.

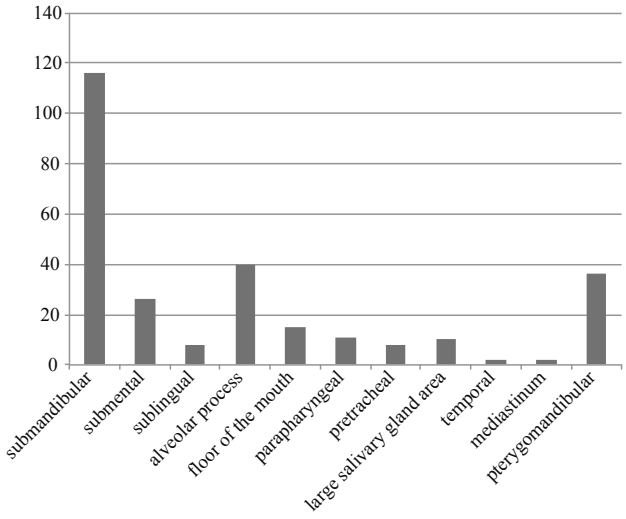

Graph 2: Affected areas.

employed adults plus 11 children, 10 students, 24 retired persons, 10 disability pension recipients, and 7 women on maternity/parent leave. The mean length of stay was 8 days, median 7 days. The shortest length of stay was 2 days: this concerned 3 patients who, after their health had improved, demanded immediate discharge from the hospital to home care at their own risk and were discharged after signing the treatment refusal form. The longest stay was 62 days: this concerned a polymorbid patient in whom cellulitis was complicated by mediastinitis. The mean time from the first symptoms to patient admission to the ward was 5 days, median 4 days (during that time the patients usually expected their health to improve spontaneously or they were treated by other health centres and by inadequate methods). In some cases the patients came to this Department only three weeks after the first symptoms of the disease.

The maxillo-facial abscess largely affected the submandibular area (Graph 2). More than one maxillo-facial space was affected in a number of patients. Odontogenic aetiology, which was the most frequent cause of the cellulitis, was identified in 173 (88.7%) patients. In 9 cases the cellulitis was caused by complicated purulent sialoadenitis and in 3 cases, by complications of purulent lymphadenitis. In isolated cases, the cellulitis was due to unrecognised mandibular fracture, tumour or furuncle. From our patients' health assessment we concluded that only 65 (33.3%) patients were free of any complicating systemic disease. A total of 40 (20.5%) patients had been treated for cardiovascular diseases and 22 (11.3%) patients were diabetics. Among those 22 diabetic patients, diabetes mellitus had not been recognised in 3, and associated congenital pancreatic atrophy was diagnosed in a 16 year old diabetic girl. Drug abuse, including intravenous narcotics, was admitted by 5 patients. None of the patients was HIV positive. Where patients with decompensated systemic diseases were involved, appropriate specialists, mostly diabetologists, internal medicine specialists or rheumatologists, were consulted regarding the therapy.

The majority of patients 194 (99.5%) complained of pain and oedema in the affected anatomic area at the time of admittance. Jaw contracture of various degrees was the next frequent (153, 78.5%) sign of cellulitis, followed by swallowing problems – odynophagia (125, 63.9%) and increased body temperature (117, 60.0%). Respiratory problems of various degrees were recorded in 10 patients. Isolated cases of neck movement disorders (2×) and dysphonia (1×) were observed (Graph 3).

In addition to the basic biochemical parameters, C-reactive protein levels, glycaemia, and blood counts were measured in all patients on the day of admission. Statistical analysis provides medium strong correlations between elevated body temperature and the CRP level (r = 0.27) and between body temperature and the leukocyte count (r = 0.26). A high correlation, however, was identified between the leukocyte count and the CRP level (r = 0.43). No correlation between the duration of the cellulitis treatment and the leukocyte count was observed (r = 0.21). A medium

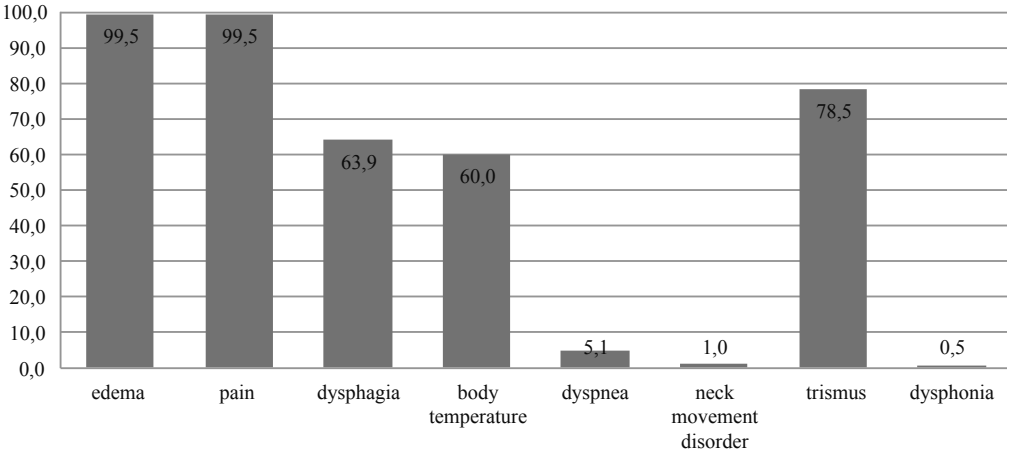

Graph 3:
The most frequent signs of cellulitis (%).

dependence of the duration of the treatment on the CRP level was found (r = 0.34).

Ultrasound examination and computed tomography were indicated in 20.5% and 12.8% of patients, respectively, within the examination on admission. In the remaining patients, cellulitis was diagnosed and therapy indicated based on clinical examination and a panoramic photograph of the jaws. Our group included 23 (11.8%) patients who reported an allergy to penicillin.

Antibiotics used within the cellulitis therapy were selected based on clinical condition severity and disease development. All antibiotics were administered intravenously. Where the results of bacteriological culture analysis were not available, the antibiotics were selected empirically. Ampicillin potentiated with clavulanic acid or cefuroxim was used in monotherapy. Where two different antibiotics were used in combination, one of the above antibiotics was usually combined with metronidazole. Three antibiotics in combination, viz. two from those mentioned above plus gentamicin, were used in the most severe cases. In patients with premonitory signs of inflammation. After obtaining the results of bacteriological analysis, the efficacy of the empirically selected antibiotics was assessed based on the antibiogram. Medication had to be changed only in those patients who stayed at the intensive care unit longer than 5 days after surgery (see Table 1 for details).

A total of 74 (38.0%) patients were treated conservatively (i.e. incision was unnecessary).

The necessity of intensive conservative treatment with parenteral antibiotics led to increased number of inpatient cases in our cohort of patients. Also the possibility of early surgical intervention when needed could be guaranteed when the patient is in the hospital.

Surgery was performed in 121 (62.1%) patients. This included intraoral incision (43 patients, who constituted 35.5% of the surgically treated patients and 22.1% of all patients included in the group) and revision and drainage of the maxillo-facial space from external access (78 patients, who constituted 64.5% of the surgically treated patients and 40.0% of all patients included in the group) – see Graph 4. Extractions of the teeth which caused the disease are not included among the surgeries. From among the surgically treated patients, 93 (76.9%) were operated on the day of admission, the remaining patients, during the first to fourth day of stay at the hospital. Two patients who were treated for severe necrotizing fasciitis were subjected to a series of surgeries. Fourteen patients were transferred to the intensive care unit after the surgery. A total of 9 patients were ventilated for 24–48 hours. In another 4 patients in very severe condition, the time of artificial lung ventilation was longer than 48 hours, temporary tracheotomy was performed after the surgery, and the patients were decanulized only before dismission (data from those patients are summarised in Table 1). For patients in whom cellulitis was complicated by mediastinitis, the surgery was performed in cooperation with a thoracic surgeon. The surgical revision of all adjacent spaces was indicated in case of phlegmone. Upper mediastinotomy was performed upon mediastinal spreading. Thoracic surgeon took part in involvement of deeper mediastinal structures. Complications in the patient group included

Tab. 1: ICU patients characteristics.

Gender	**Female**	**Male**	**Male**	**Male**
Age	57	62	35	43
General health	Corticosteroids	Diabetes	Coxarthrosis	Diabetes Pancreatitis Hepatopathy
Aetiology	Odontogenic	Odontogenic	Odontogenic	Odontogenic
Body temperature	39.4	36.6	39.1	35.6
Leukocytes	20.01	22.3	16.88	7.84
CRP	254	370	278	204
APV	**13**	**19**	**4**	**8**
ICU	**17**	**25**	**12**	**15**
Total duration of stay	**31**	**62**	**34**	**25**
Complications	Sepsis MODS	Mediastinitis Pneumonia	Pleural effusion Effusion	Pleural effusion Mediastinitis Pneumonia
Microbiology	Streptococcus spp.	Staphylococcus spp. Enterococcus spp. Peptosterptococcus spp. Peptostreptococcus spp. Bacteroides spp.	Staphylococcus spp. Peptostreptococcus spp. Bacteroides spp. Propionibacterium spp. Enterobacter spp.	Burkholderia spp. Stenotrophomonas spp. Candida albicans Candida tropicalis

mediastinitis, pneumonia and pleural effusion in 2 patients (1.0%). Signs of sepsis were diagnosed in 4 (2.1%) patients. The multiple organ dysfunction syndrome developed in one (0.5%) patient who had been on long-term corticosteroid therapy for another disease. None of the patients in the study group died. Permanent consequences of the cellulitis treatment only included scarring on the skin and the loss of teeth that were the root of the disease.

The results of microbiological examination were available retrospectively for 74 patients. The culture was negative in 12 (16.2%) patients and positive in 62 (83.8%) patients. Various species of the bacterial genera *Streptococcus*, *Staphylococcus*, *Peptostreptococcus*, *Propionibacterium*, *Haemophilus*, *Stenotrophomonas*, *Burkholderia*, *Enterobacter*, *Klebsiella*, *Pseudomonas*, *Escherichia*, *Lactobacillus*, *Prevotella*, *Neisseria*, *Actinomyces*, *Veillonella*, *Fusobacterium*, *Enterococcus* were identified. Yeasts of the genus *Candida* were also identified in 3 cases (*C. albicans* 2×, *C. tropicalis* 1×). Somewhat atypical microbiological results were obtained for 4 patients (Table 1). A triazole antimycotic (fluconazole) was administered systemically to patients in whom mycotic infection had been identified. Patients with the cervico-facial form of actinomycosis were treated with benzyl-penicillin. An overview of the microbiological findings is presented in Graph 5.

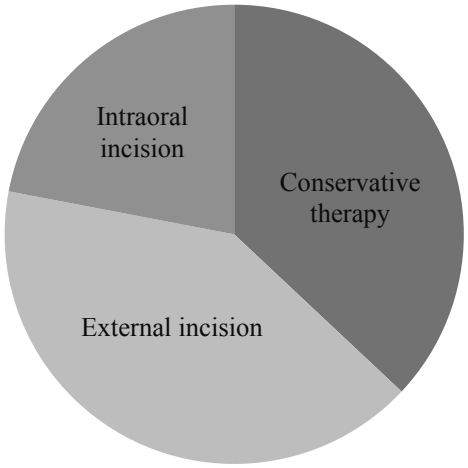

Graph 4: Cellulitis therapy modalities.

Discussion

The results of this study of cellulitis patients were compared to those of similar studies from other hospitals, where streptococci, staphylococci and prevotellae were identified as the major pathogenic microorganisms (2, 3, 5, 7–15). This is borne out by our observations. However, while some papers (3, 5, 12, 14) mention *Klebsiella pneumoniae* as a significant infectious agent for cellulitis in diabetics, we observed this microorganism only twice in our patient group, and those 2 individuals were not diabetics. The frequency at which the various maxillo-facial spaces were affected was also in line with published data (1, 3, 6, 10, 11, 16, 17). Neither the therapeutic procedures nor the types of the empirically selected antibiotics were different either.

The frequency of severe complications, especially mediastinitis and septic conditions, was similar to that observed by Czech otorhinolaryngologists (6), who examined a group of 634 patients, among whom mediastinitis was present in 6.6% and mortality was 0.6%.

According to some authors (7), cellulitis more frequently affects individuals from socially and economically disadvantaged populations. This conclusion was not confirmed by our study. In our group, there were only 17 unemployed as already mentioned. We explain this, among other factors, by the generally insufficient information and motivation and

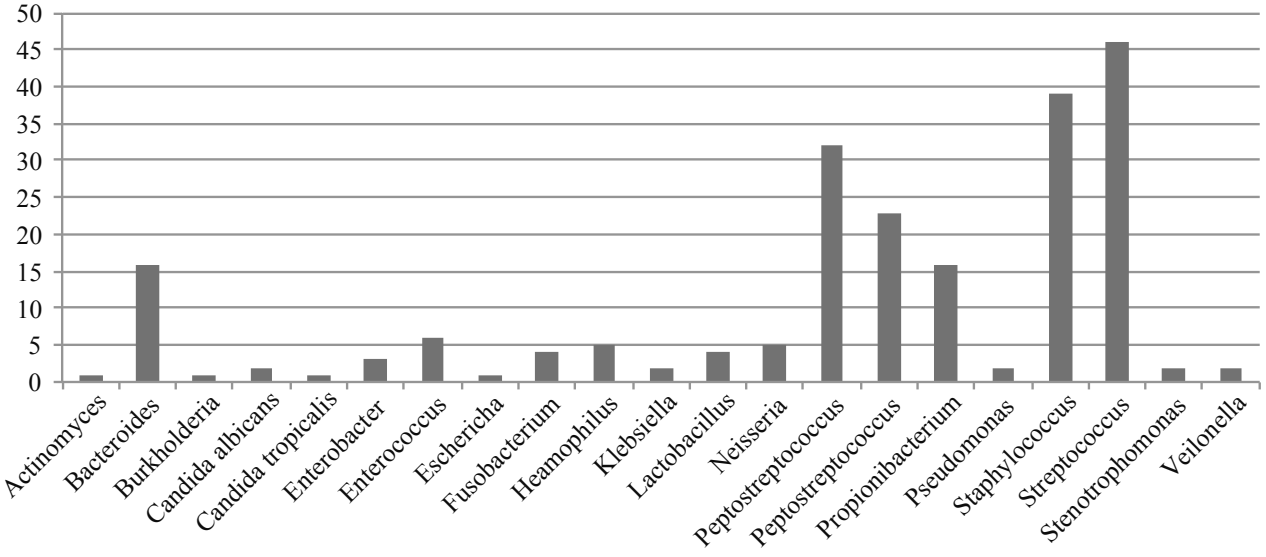

Graph 5: Microorganisms in the cultures.

the associated poor level of oral hygiene and hence, poor oral health, still existing in a large fraction of the Czech population.

Modern imaging methods such as magnetic resonance and positron emission tomography are quite frequently included among examination algorithms for patients with cellulitis in developed countries (3, 5, 6, 12, 18). Although those techniques are relatively well available and their use in cellulitis diagnosis is feasible in the Czech health sector as well, routine diagnosis of cellulitis at our department remains based on proven classical imaging methods, which are thus far more readily available and less expensive.

We frequently encountered situations where the dental practitioners hesitated and failed to resolve to extract the target tooth, even though the diagnosis of cellulitis was quite clear at that time. It is clear that this "let's wait" approach, consisting in administration of oral antibiotics and trepanation of the tooth, cannot be successful in cases of developing or fully developed cellulitis (in fact, postponing the tooth extraction procedure till the patient's conditions improves appreciably is warranted only in exceptional cases where the tooth is actually inaccessible). Only timely elimination of the cause associated with incision and drainage of the focus of the abscess (if present) will prevent further propagation of infection to the surrounding anatomic areas and reduce the time of treatment appreciably. This requires perfect knowledge of the topographic-anatomic situation in the maxillo-facial spaces and areas where the inflammation exudate is typically present. This is based on the clinical finding and ultrasound examination. Computed tomography may be of assistance in this as well.

Conclusion

In conclusion, cellulitis continues to be a frequent and rather severe disease of odontogenic origin in the maxillo-facial area. Its incidence can apparently be reduced only by fundamental "oral health" improvement among the Czech population as a whole, and also by adequate, i.e. timely and good quality treatment of teeth with "banal" diseases, particularly caries and its complications, which unless adequately treated as outlined above, result in infection transfer to the surrounding tissues and sometimes in the induction of serious diseases endangering patient health and life.

Acknowledgements

This study was conducted within the PRVOUK P37/13 Project.

References

1. Peterson LJ. Contemporary management of deep infections of the neck. J Oral Maxillofac Surg 1993 April; 51(3): 226–31.
2. Poeschl PW, Spusta L, Russmueller G, et al. Antibiotic susceptibility and resistance of the odontogenic microbiological spectrum and its clinical impact on severe deep space head and neck infections. Oral Surg Oral Med Oral Pathol Oral Radiol Endod 2010 August; 110(2): 151–6.
3. Boscolo-Rizzo P, Da Mosto MC. Submandibular space infection: a potentially lethal infection. Int J Infect Dis IJID 2009 May; 13(3): 327–33.
4. Santos Gorjón P, Blanco Pérez P, Morales Martín AC, et al. Deep neck infection. Review of 286 cases. Acta Otorrinolaringológica Esp 2012 February; 63(1): 31–41.
5. Lee J-K, Kim H-D, Lim S-C. Predisposing factors of complicated deep neck infection: an analysis of 158 cases. Yonsei Med J 2007 February 28; 48(1): 55–62.
6. Celakovsky P, Kalfert D, Tucek L, et al. Deep neck infections: risk factors for mediastinal extension. Eur Arch Oto-Rhino-Laryngol 2014 June; 271(6): 1679–83.
7. Agarwal AK, Sethi A, Sethi D, Mrig S, Chopra S. Role of socioeconomic factors in deep neck abscess: A prospective study of 120 patients. Br J Oral Maxillofac Surg 2007 October; 45(7): 553–5.
8. Al-Qamachi LH, Aga H, McMahon J, Leanord A, Hammersley N. Microbiology of odontogenic infections in deep neck spaces: a retrospective study. Br J Oral Maxillofac Surg 2010 January; 48(1): 37–9.
9. Boyanova L, Kolarov R, Gergova G, et al. Anaerobic bacteria in 118 patients with deep-space head and neck infections from the University Hospital of Maxillofacial Surgery, Sofia, Bulgaria. J Med Microbiol 2006 September; 55(Pt 9): 1285–9.
10. Har-El G, Aroesty JH, Shaha A, Lucente FE. Changing trends in deep neck abscess. A retrospective study of 110 patients. Oral Surg Oral Med Oral Pathol 1994 May; 77(5): 446–50.
11. Hasegawa J, Hidaka H, Tateda M, et al. An analysis of clinical risk factors of deep neck infection. Auris Nasus Larynx 2011 February; 38(1): 101–7.
12. Huang T-T, Liu T-C, Chen P-R, Tseng F-Y, Yeh T-H, Chen Y-S. Deep neck infection: analysis of 185 cases. Head Neck 2004 October; 26(10): 854–60.
13. Krautsevich L, Khorow O. Clinical aspects, diagnosis and treatment of the phlegmons of maxillofacial area and deep neck infections. Otolaryngol Pol Pol Otolaryngol 2008; 62(5): 545–8.
14. Rao DD, Desai A, Kulkarni RD, Gopalkrishnan K, Rao CB. Comparison of maxillofacial space infection in diabetic and nondiabetic patients. Oral Surg Oral Med Oral Pathol Oral Radiol Endod 2010 October; 110(4): e7–12.
15. Sakaguchi M, Sato S, Ishiyama T, Katsuno S, Taguchi K. Characterization and management of deep neck infections. Int J Oral Maxillofac Surg 1997 April; 26(2): 131–4.
16. Bakir S, Tanriverdi MH, Gün R, et al. Deep neck space infections: a retrospective review of 173 cases. Am J Otolaryngol 2012 February; 33(1): 56–63.
17. Smith JL, Hsu JM, Chang J. Predicting deep neck space abscess using computed tomography. Am J Otolaryngol 2006 August; 27(4): 244–7.
18. Umeda M, Minamikawa T, Komatsubara H, Shibuya Y, Yokoo S, Komori T. Necrotizing fasciitis caused by dental infection: a retrospective analysis of 9 cases and a review of the literature. Oral Surg Oral Med Oral Pathol Oral Radiol Endod 2003 March; 95(3): 283–90.

Received: 16/06/2015
Accepted in revised form: 09/09/2015

Corresponding author:

Helena Doležalová, MD, Department of Dentistry, Teaching Hospital Hradec Králové, Sokolská 581, 500 05 Hradec Králové, Czech Republic; e-mail: helena.dolezalova@fnhk.cz

ORIGINAL ARTICLE

NON-INVASIVE OCULAR RIGIDITY MEASUREMENT: A DIFFERENTIAL TONOMETRY APPROACH

Efstathios T. Detorakis[1,2], *Emmanuela Tsaglioti*[1], *George Kymionis*[1,2]

Institute of Vision & Optics, University of Crete, Greece[1]; Department of Ophthalmology, University Hospital of Heraklion, Greece[2]

Summary: Purpose: Taking into account the fact that Goldmann applanation tonometry (GAT) geometrically deforms the corneal apex and displaces volume from the anterior segment whereas Dynamic Contour Tonometry (DCT) does not, we aimed at developing an algorithm for the calculation of ocular rigidity (OR) based on the differences in pressure and volume between deformed and non-deformed status according to the general Friedenwald principle of differential tonometry. Methods: To avoid deviations of GAT IOP from true IOP in eyes with corneas different from the "calibration cornea" we applied the previously described Orssengo-Pye algorithm to calculate an error coefficient "C/B". To test the feasibility of the proposed model, we calculated the OR coefficient (r) in 17 cataract surgery candidates (9 males and 8 females). Results: The calculated r according to our model (mean ± SD, range) was 0.0174 ± 0.010 (0.0123–0.022) mmHg/μL. A negative statistically significant correlation between axial length and r was detected whereas correlations between r and other biometric parameters examined were statistically not significant. Conclusions: The proposed method may prove a valid non-invasive tool for the measurement method of OR, which could help in introducing OR in the decision-making of the routine clinical practice.

Key words: *Cornea; Sclera; Ultrasonography*

Introduction

Ocular Rigidity (OR) is an important property of the ocular tissues associated with their resistance to mechanical deformation (1). From a purely mathematical standpoint, OR refers to the correlation between pressure and volume in a chamber filled with incompressible content (1–4). This mathematical correlation is affected by the elastic properties of the chamber walls (1–4). However, in the case of the eyeball, which is also filled with incompressible content (aqueous humor and gel-like vitreous body), rigidity is affected by not only the elastic properties of the sclera and cornea but also by other factors, such as the vascular uveal layer (5). The latter displays a dynamic change in its elastic properties due to constant changes in the amount of blood contained in uveal vessels in response to a variety of physiological factors, such as the cardiac cycle, respiratory movements or intraocular pressure (IOP) changes (6). Moreover, the internal compartmental architecture of the eyeball, organized as anterior segment (filled by dynamically flowing queous humor) and posterior segment (filled by the more static vitreous body gel), complicate its bio-mechanical behaviour, which has accordingly been described as poro-elastic, rather than elastic (7). In the case of the cornea, bio-mechanical behaviour also includes a visco-elastic or anisotropic element, implying that that the rate at which a load is applied changes the measured value for cornea's Young's modulus (7–9). The latter describes the resistance of corneal tissue to mechanical deformation and corresponds to the relation between tensile strain and tensile stress of corneal tissue (9). Reported corneal Young's modulus values range from 0.159 MPa to 57 Mpa (mean 0.29 ± 0.06 Mpa) (7–9), reflecting the complexity of ex-vivo corneal bio-mechanical behaviour.

Several attempts have so far been made to measure OR (1, 10–13). The initial land-mark studies of Friedenwald in 1937, who employed a differential tonometry methodology (using indentation or indentation and applanation tonometry) in human cadaver eyes, have resulted in a purpose-designed chart providing an OR coefficient (on the average 0.0215 mmHg/μL) (1). According to the Friedenwald model, the rigidity coefficient (K) may be calculated as:

$$K = \frac{\log IOP_1 - \log IOP_2}{V_1 - V_2}$$

Where P_1 and P_2 as well as V_1 and V_2 refer to respective values of intraocular pressure and volume (1). However, this approach has received criticism because the conditions in living human eyes are notably different from those in cadaveric eyes due to blood circulation and the lack of

ACTA MEDICA (Hradec Králové) 2015; 58(3): 92–97
http://dx.doi.org/10.14712/18059694.2015.99

post-mortem connective tissue changes (11). Other researchers have since then attempted to measure OR using a variety of methodologies (10–13). More recently, Pallikaris et al. have reported accurate rigidity measurements by inserting a manometric catheter into the anterior chamber and directly measuring pressure-volume changes (11). However, this approach is invasive (requires a surgical intervention) and thus cannot be used in the every-day clinical practice. In fact, an important obstacle in including OR in the routine clinical decision-making has been the lack of a simple, accurate and, more importantly, non-invasive methodology for its quantitative assessment, despite the fact that OR may be involved in a variety of clinical situations, such as glaucoma, age-related macular degeneration (AMD) or presbyopia (3). Based on this point, we aimed at developing such a methodology by mathematically analyzing differential tonometry readings between applanation and non-applanation tonometers in association with other clinical parameters, all easily recordable in a non-invasive manner.

Material and Methods

This study was conducted at the Department of Ophthalmology of the University Hospital of Heraklion, in Crete, Greece and the protocol was approved by the local ethical committee. Cataract candidate patients were included in the study. A mathematical algorithmic tool to measure OR based on Friedenwald's principle but using ophthalmic parameters recorded in a non-invasive manner was developed. The tool was examined in a group of cataract surgery candidates. Eyes with a history of trauma, surgical procedures or inflammatory conditions as well as eyes with glaucoma and a history of anti-glaucomatous eye drop use were excluded. Moreover, eyes with corneal dystrophies or other ocular surface conditions, such as pterygium, or posterior segment abnormalities, such as staphylomas, were also excluded. None of the eyes included had astigmatism over 3.00D and the spherial equivalent was below 8.00D in all cases. Overall, 17 patients (9 males and 8 females) were included in the study.

Theoretical concept for the formation of the algorithmic tool

Taking into account that the basic definition of OR relates with the association between pressure and volume changes in the eyeball, we explored the possibility to take advantage of the "delta", i.e. the difference (ΔIOP) between applanation (GAT) and non-applanation (DCT) tonometry, in association with the volume displaced during the applanation phase of GAT. The latter depends on a modified "Imbert-Fick" concept, according to which the pressure (P) within a sphere with ideally elastic and thin walls equals to the force necessary to applanate a part of the sphere (W) divided by the area applanated (A), whereas the force necessary to distort the cornea (B) and surface tension (S) are also involved: $W + S = P \times A + B$ (14). In the case of DCT, the Pascal principle applies, referring to the equality of forces created by actual IOP, capillary traction and ocular rigidity on the anterior corneal surface (2). The basic difference between the 2 methods refers to the lack of applanation of the anterior corneal surface, thus lack of induced corneal deformation and respective volume displacement in the case of DCT (2). During GAT the displaced volume corresponds to an ellipsoid cup (Figure 1). By applying the general ellipsoid equation (15) of

$$\frac{x^2}{a^2}+\frac{y^2}{b^2}+\frac{z^2}{c^2}=1$$

in which a, b and c refer to the width along the x-, y- and z-axes, respectively, whereas X(0,0,x) is a point on the ellipsoid surface such as −c × c, the ellipsoid cup volume can been calculated by a standard calculating machine (16) as:

$$V=\pi ab\left(\frac{2c}{3}-x+\frac{x^3}{3c^2}\right)$$

To apply the general Friedenwald principle of differential pressure and volume we assumed that the initial eye volume corresponds with the corneal status during DCT (i.e. non-deformed) whereas the final ocular volume corresponds with the corneal status during GAT (i.e. with corneal deformation and associated volume displacement). Moreover, taking into account the lack of deformation in DCT, we assumed that DCT IOP reading approximates true IOP without the need of further corrections. However, according to the previously published model of Orssengo-Pye (17), GAT IOP readings equal true IOP when corneal parameters are in agreement with the geometrical characteristics of the so-called "calibrated cornea", such as CCT of 520 μm and mean external radius of curvature of 7.8 mm. To correct for deviations of GAT IOP from true IOP in eyes with corneas different from the "calibration cornea" we applied the Orssengo-Pye algorithm (17):

$$IOP_P=\frac{IOP_G}{C/B}$$

In the error coefficient "C/B" B corresponds to the IOP_G of the calibrated cornea and C corresponds to the IOP of the measured cornea (17). To calculate B and C the following equations were applied (17):

$$B=\frac{0.6\cdot\pi\cdot R\cdot\left(R-\frac{t}{2}\right)\cdot\sqrt{1-\nu^2}}{t^2}$$

$$C=\frac{\pi\cdot R\cdot\left(R-\frac{t}{2}\right)^2\cdot(1-\nu)}{A\cdot t}$$

Where R corresponds to the anterior corneal curvature, t corresponds to the central corneal thickness (CCT), ν is the Poisson's index for the cornea (0.49) and A is the area of applanation. Instead of a CCT of 520 μm as originally proposed by Orssengo-Pye we used the mean CCT of patients included in this study (549 μm). In accordance with the initial differential tonometry equation described by Friedenwald but incorporating the error coefficient C/B for the deviation of the measured cornea for the calibrated cornea in GAT IOP, as well as the mean corneal Young's modulus (E) previously reported (9), and thus measured "r" using the following algorithm:

$$r = [(IOP_{Pascal} - IOP_{Goldmann} / \Delta V) \times C/B] \times E$$

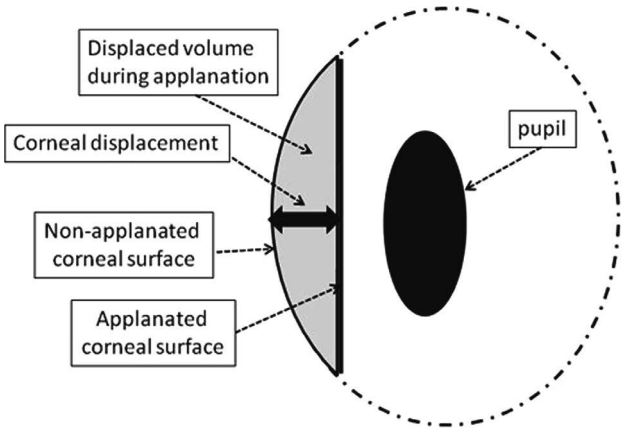

Fig. 1: Applanated and non-applanated corneal surfaces in GAT with respective ellipsoid cup volume displacement.

Clinical application of the proposed algorithm

All patients underwent a typical preoperative clinical examination, including IOP measurements by both Goldmann Applanation Tonometry (GAT) and Dynamic Contour Tonometry (DCT), ultrasonic axial length (AL) and anterior corneal surface curvature measurements, ultrasonic central corneal thickness (CCT) measurement as well as measurements of the maximal eyeball diameter (corresponding to the equatorial region) along both transverse (TD) and coronal (CD) planes. DCT (SMT Swiss Microtechnology AG, Port, Switzerland) was performed immediately after instillation of proparacaine eye drops in the examined eyes (3 readings Q1–Q3, as per manufacturer instructions were taken and the mean value recorded). GAT was then performed (after the application of a fluorescein strip at the lower conjunctival fornix). Five GAT measurements were taken in eaqch eye and the average was recored as the GAT IOP. CCT, AL, TD and CD were measured with the Alcon OcuScan® RxP Ophthalmic Ultrasound System (Alcon laboratories, Alcon, Irvine, CA, USA), employing a 20 Mhz probe for CCT,

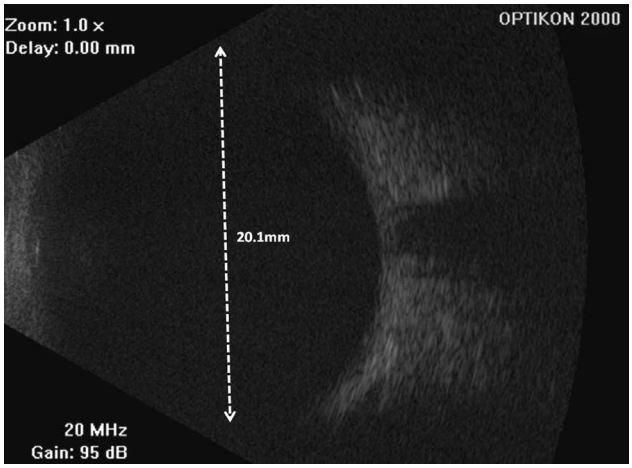

Fig. 2: Ophthalmic B-scan image with measurement of maximal (equatorial) globe diameter (in this case 20.1 mm, shown with dashed lines), along the coronal plane.

(with a resolution of ± 1 μm and an accuracy of ± 5μm) and a 10 Mhz probe (with a resolution of ± 0.1mm and a theoretical accuracy of ± 0.05mm) for AL, TD and CD. TD and CD were recorded using a B-scan mode of ultrasonic imaging by obtaining a cross-sectional image of the eye at the transverse (nasal-temporal diameter) and coronal (superior-inferior diameter) planes, respectively. Measurements were taken with the built-in measurement tool by placing the measurement cursors along the largest diameter of the examined eye, on the transverse and coronal planes (Figure 2). For all ultrasonic parameters, which were performed by the same experienced examiner (ET), 10 successive measurements were taken and the mean was recorded.

Statistical analysis

The examination correlations between the parameters recorded was performed with Pearson's bivariate correlation coefficient. Statistical significance was set at 0.05. Statistical analyses were performed with the statistical package SPSS 8.0 (SPSS, Chicago, IL, USA).

Results

Measurements (mean ± SD, range) of the recorded parameters in the group of patients studied is presented in Table 1. The application of the algorithm mentioned in the case series included in this feasibility study rendered an index (r) of corneal rigidity of 0.0174 ± 0.010 (0.0123–0.022) mmHg/μL. The delta recorded was 1.78 ± 0.71 (−0.10–2.08) mmHg. The correlation between delta and r was statistically significant (Pearson's bivariate correlation coefficient 0.803, $p \approx 0.00$) (Figure 3). A negative correlation between AL and r was detected, although at a borderline statistical signficance level (Pearson's bivariate correlation coefficient −0.482, $p = 0.048$) (Figure 4). On the contrary, the corre-

Tab. 1: Parameters recorded with mean, SD and range values.

Parameter	Mean	SD	Range
AL (mm)	23.63	1.16	21.19–25.84
R (mm)	7.82	0.29	7.44–8.48
CCT (μm)	548.94	37.80	462–594
Goldmann (mmHg)	16.29	3.46	10–20
Pascal (mmHg)	16.25	3.48	11.4–22.8
Nasal-Temporal diameter (mm)	18.95	0.98	17.56–20.60
Superior-Inferior diameter (mm)	18.81	0.94	17.33–20.45
Ocular Rigidity	0.0173	0.0070	0.0080–0.0329
ΔIOP (mmHg)	1.78	0.71	0.8–3.3

lation between r and the the vertical or horizontal maximal diamterers of the eyeball was statistically not significant (Pearson's bivariate correlation coefficient). Moreover, the correlations between CCT, corneal curvature, DCT or GAT was statistically not significant (Pearson's bivariate correlation coefficient).

Discussion

This study examined the feasibility of using "delta" as a metric for the calculation of corneal rigidity, based on the mathematical analysis of various biometric indices. Results imply that "delta" may be used to calculate a coefficient for OR (r) in a non-invasive manner applicable in the every-day clinical practice.

The accurate non-invasive measurement of OR has been the target of various research projects so far (1, 3, 7, 18). Calculating "r" for a particular eye is very important since "r" varies considerably between eyes and this variation may have clinical implications for the course of several conditions, such as glaucoma (12), presbyopia (3) or AMD (19). Although in the case of glaucoma there have been reports for the assessment of ocular biomechanical properties through the use of modalities such as the Ocular Response Analyzer (ORA), so far results are inconclusive (20). In the case of ORA, the association between corneal hysteresis and the OR or Young's modulus of the cornea is unclear and hysteresis has been shown to decrease during aging, when the cornea is known to stiffen, as well as to decrease after the cornea has been stiffened by cross-linking techniques (3, 20). Nevertheless, the accurate assessment of OR may also be of value in the case of pseudoexfoliation syndrome and exfoliation glaucoma, in which the biomechanical behaviour of affected tissues may be changed though the accumulation of pseudoexfoliative material *per se* or through alterations in blood supply (21–23). In a previously published paper by Liu & Roberts, a model of simulation of corneal biomechanical behaviour was proposed and it was shown that variations in corneal biomechanics, expressed by differences in corneal Young's modulus, may actually affect IOP to a greater extent than corneal thickness or curvature (24). Furthermore, the use of corneal cross-linking in the management of keratoconus and other corneal conditions such as post-LASIK ectasia may also have implications for OR due to significant changes in corneal biomechanical properties (25) and the introduction of a non-invasive quantitative method to assess OR as the

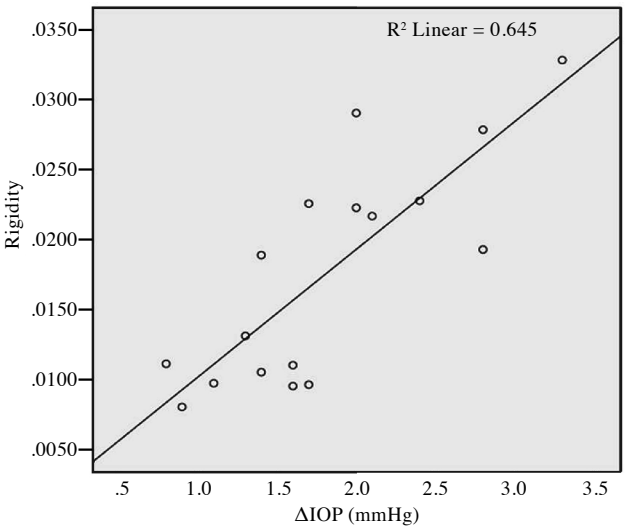

Fig. 3: Correlation between ΔIOP and Rigidity (r) in the group of patients studied.

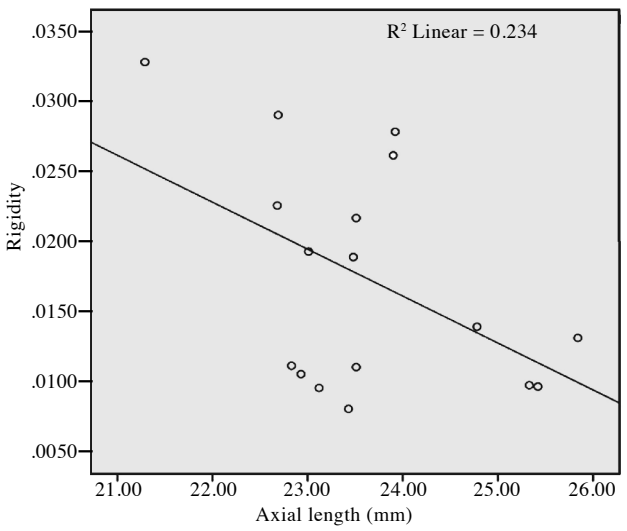

Fig. 4: Correlation between AL and Rigidity (r) in the group of patients studied.

one described in the present study, could provide important clinical information.

Moreover, it has become evident that the elastic properties of the ocular walls, especially those of the cornea, affect significantly the accuracy of tonometric methods, such as the indentation (SchiÖtz) tonometry (2, 14). Although GAT was initially considered to be immune from such effects, it soon became evident that it is was significantly affected by a variety of corneal parameters, including CCT (26), corneal curvature (27), corneal astigmatism (28), AL (29) or even the bio-mechanical properties of corneal collagen, most of them related with OR (2). DCT may be less affected by CCT, compared with GAT, however it may in fact be more affected by corneal curvature, since during DCT the concave surface of the tonometer head (which has a pre-determined radius of curvature corresponding to the average corneal curvature) has to conform geometrically with the anterior corneal surface, which varies in curvature between different eyes (2). Nevertheless, the fundamental difference between GAT and DCT lies in the event of applanation in GAT and respective lack of applanation in DCT (2). The average volume displaced during applanation has been reported to be 0.5 μL, but it differs between different eyes, depending on corneal geometry (the volumetric displacement in applanation tonometry of a cornea with a radius of curvature of 4.5 mm has been reported to be 0.995 ml, while that of a cornea with a radius of 15.5 mm has been reported to be 0.281 ml) (3, 30). The methodology proposed in this study takes advantage of this volume, which is calculated in a customized fashion for the individual eye examined, based on a three-dimensional ellipsoid model of the eyeball. A modified concept of differential tonometry, based on the originally proposed model by Friedenwald for SchiÖtz tonometry performed with 2 different weights (or for SchiÖtz and GAT tonometries), is then applied between GAT and DCT.

The average "r" calculated for the eyes included in this case series is very close to previously reported "r" scores, calculated with other methodologies in previous studies, such as those by Friedenwald (0.0215) (1), Goldmann (0.020) (13), Drance (0.0217) (10), Agarwal (0.0217) (12) and Pallikaris (0.0126) (11). Moreover, a negative association between AL and r has also been previously reported (4). These consistencies enhance the validity of the proposed methodology. On the other hand, weaknesses of the present study are the small number of patients included, the requirement for the availability of a non-applanation tonometer and the lack of a purpose-designed independent validation method for the calculation of "r" applied on the same case series. Accordingly, a further step in the examination of the validity of the methodology proposed could be the comparison of results with results from a different method of OR measurement performed on the same series of eyes. Moreover, assumptions were also employed in the approach described in this study, such as the fact that DCT IOP corresponds with the "true" IOP in the non-deformed corneal status whereas results may better describe corneal rigidity, rather than ocular rigidity, since deformation corresponds to corneal geometry. It could also be argued that since the volume of the anterior chamber is around 250 μl, and the volume of the anterior chamber displaced by Goldmann tonometry is around 0.5 μl (3), i.e. 0.2% of the total volume, it may be hard to predict ocular rigidity changes based on the volume displaced by Goldmann tonometry alone. However, previously published models for the calculation of OR are also based on very small changes in ocular geometry (e.g. a reduction in AL of 14.2–23 μm) (18), implying that the mathematical tools employed may have the power to assess OR based on such small deviations.

The obvious advantage of the present methodology is its non-invasive nature, which enables its application in the every-day clinical practice. A previous study attempted to measure OR by examining changes in AL (associated with ocular volume changes) caused by the oral administration of acetazolamide (500 mg), which would later result in a respective IOP reduction (18). Although this methodology may also be considered non-invasive, it requires, the systemic administration of acetazolamide (which may be contra-indicated in some patients) and may be more time-consuming than the present approach, which could render its application difficult in a busy clinical setting. The methodology presented in this study overcomes these obstacles and, if proved valid, may be a useful clinical tool in the customized assessment of OR, enabling its active involvement in the decision making for a variety of clinical situations.

References

1. Friedenwald JS. Tonometer calibration; an attempt to remove discrepancies found in the 1954 calibration scale for Schiotz tonometers. Trans Am Acad Ophthalmol Otolaryngol 1957; 61: 108–222.
2. Detorakis ET, Arvanitaki V, Pallikaris IG, Kymionis G, Tsilimbaris MK. Applanation Tonometry versus Dynamic Contour Tonometry in Eyes Treated with Latanoprost. J Glaucoma 2010; 19: 194–198.
3. Detorakis ET, Pallikaris IG. Ocular rigidity: biomechanical role, in vivo measurements and clinical significance. Clin Experiment Ophthalmol 2013; 41: 73–81. doi: 10.1111/j.1442–9071.2012.02809.x. Epub 2012 Jul 2. Review.
4. Dastiridou AI, Ginis H, Tsilimbaris M, et al. Ocular rigidity, ocular pulse amplitude, and pulsatile ocular blood flow: the effect of axial length. Invest Ophthalmol Vis Sci 2013 Mar 1; 54: 2087–92.
5. Friberg TR, Lace JW. A comparison of the elastic properties of human choroid and sclera. Exp Eye Res 1988; 47: 429–436.
6. Hommer A, Fuchsjäger-Mayrl G, Resch H, Vass C, Garhofer G, Schmetterer L. Estimation of ocular rigidity based on measurement of pulse amplitude using pneumotonometry and fundus pulse using laser interferometry in glaucoma. Invest Ophthalmol Vis Sci 2008; 49: 4046–50.
7. Detorakis ET, Drakonaki EE, Tsilimbaris MK, Pallikaris IG, Giarmenitis S. Real-time ultrasound elastographic imaging of ocular and periocular tissues: a feasibility study. Ophthalmic Surg Lasers Imaging 2010; 41: 135–41.
8. Detorakis ET, Drakonaki EE, Ginis H, Karyotakis N, Pallikaris IG. Evaluation of iridociliary and lenticular elasticity using shear-wave elastography in rabbit eyes. Acta Medica (Hradec Králové) 2014; 57: 9–14.

9. Hamilton KE, Pye DC. Young's modulus in normal corneas and the effect on applanation tonometry. Optom Vis Sci 2008; 85: 445–50.
10. Drance SM. The coefficient of scleral rigidity in normal and glaucomatous eyes. Arch Ophthalmol 1960; 63: 668–74.
11. Pallikaris IG, Kymionis GD, Ginis HS, Kounis GA, Tsilimbaris MK. Ocular rigidity in living human eyes. Invest Ophthalmol Vis Sci 2005; 46: 409–14.
12. Agrawal KK, Sharma DP, Bhargava G, Sanadhya DK. Scleral rigidity in glaucoma, before and during topical antiglaucoma drug therapy. Indian J Ophthalmol 1991; 39: 85–86.
13. Goldmann H, Schmidt T. Friedenwald's rigidity coefficient. Ophthalmologica 1957; 133: 330–335.
14. Goldmann H. Un nouveau tonomètre à aplanation [A new applanation tonometer]. Bull Mem Soc Fr Ophtalmol 1954; 67: 474–7.
15. Harris WF. Curvature of ellipsoids and other surfaces. Ophthalmic Physiol Opt 2006; 26: 497–501.
16. http://www.codecogs.com/library/maths/geometry/volume/ellipsoidal_cap.php
17. Orssengo GJ, Pye DC. Determination of the true intraocular pressure and modulus of elasticity of the human cornea in vivo. Bull Math Biol 1999; 61: 551–72.
18. Ebneter A, Wagels B, Zinkernagel MS. Non-invasive biometric assessment of ocular rigidity in glaucoma patients and controls. Eye 2009; 23: 606–611.
19. Pallikaris IG, Kymionis GD, Ginis HS, Kounis GA, Christodoulakis E, Tsilimbaris MK. Ocular rigidity in patients with age-related macular degeneration. Am J Ophthalmol 2006; 141: 611–615.
20. Shah S, Laiquzzaman M, Bhojwani R, Mantry S, Cunliffe I. Assessment of the biomechanical properties of the cornea with the ocular response analyzer in normal and keratoconic eyes. Invest Ophthalmol Vis Sci 2007; 48: 3026–3031.
21. Detorakis ET, Chrysochoou F, Paliobei V, et al. Evaluation of the acoustic function in pseudoexfoliation syndrome and exfoliation glaucoma: audiometric and tympanometric findings. Eur J Ophthalmo. 2008; 18: 71–6.
22. Detorakis ET, Koukoula S, Chrisohoou F, Konstas AG, Kozobolis VP. Central corneal mechanical sensitivity in pseudoexfoliation syndrome. Cornea 2005; 24: 688–91.
23. Detorakis ET, Achtaropoulos AK, Drakonaki EE, Kozobolis VP. Hemodynamic evaluation of the posterior ciliary circulation in exfoliation syndrome andexfoliation glaucoma. Graefes Arch Clin Exp Ophthalmol 2007; 245: 516–21.
24. Liu J, Roberts CJ. Influence of corneal biomechanical properties on intraocular pressure measurement: quantitative analysis. J Cataract Refract Surg 2005; 31: 146–55.
25. Sorkin N, Varssano D. Corneal collagen crosslinking: a systematic review. Ophthalmologica 2014; 232: 10–27.
26. Ehlers N, Bramsen T, Sperling S. Applanation tonometry and central corneal thickness Acta Ophthalmol (Copenh) 1975; 53: 34–43.
27. Mark H. Corneal curvature in applanation tonometry Am J Ophthalmol 1973; 76: 223–224.
28. Francis BA, Hsieh A, Lai MY, et al. Los Angeles Latino Eye Study Group. Effects of corneal thickness, corneal curvature, and intraocular pressure level on Goldmann applanation tonometry and dynamic contour tonometry. Ophthalmology 2007; 114: 20–26.
29. Mark H, Robbins KP, Mark TL. Axial length in applanation tonometry. J Cataract Refract Surg 2002; 28: 504–506.
30. Abdalla MI, Hamdi M. Applanation ocular tension in myopia and emmetropia. Br J Ophthalmol 1970; 54: 122–125.

Received: 17/05/2015
Accepted in revised form: 22/08/2015

Corresponding author:

Efstathios T. Detorakis, MD, PhD, FEBO, Department of Ophthalmology, University Hospital of Heraklion, 71110, Heraklion, Crete, Greece; e-mail: detorakis@hotmail.com

ORIGINAL ARTICLE

OSTEOCHONDRITIS DISSECANS OF THE KNEE IN CHILDREN AND ADOLESCENTS: OUR EXPERIENCE WITH TRANSCHONDRAL DRILLING

Haroun Hassan Shaikh, Jan Vícha, Tomáš Proček, Jaroslav Pavlata, Tomáš Kučera

Charles University in Prague, Faculty of Medicine and University Hospital in Hradec Králové, Czech Republic: Department of Orthopedic Surgery

Summary: Osteochondritis dissecans(OCD) of the knee is identified with increasing frequency in the adolescent patient. Left untreated, OCD can cause significant impairment and restriction in physical activity and development of osteoarthritis at an early age. The diagnosis of lesions of OCD can be confirmed on plain radiographs. MRI has emerged as the gold standard to evaluate the stability of the lesion and the integrity of the overlying articular cartilage. Treatment of OCD lesions depend on the stability of the lesion. Stable lesions can be treated conservatively by physical activity modification and immobilization. Unstable lesions and stable lesions not responding to conservative measures should be treated surgically. Surgical options range from arthroscopic drilling, either transarticular or extra-articular drilling for stable lesions or salvage procedures such as autologous chondrocyte transplantation (ACT), mosaicplasty to restore joint and cartilage congruency.

Keywords: *Osteochondritis dissecans; Juvenile OCD; Transarticular drilling; Knee joint*

Introduction

Osteochondritis dissecans (OCD) is a condition that affects the subchondral bone and the articular cartilage and can lead to separation of articular fragment from the underlying bone. The Research for Osteochondritis dissecans of the knee (ROCK) recently defined OCD as a focal idiopathic alteration of subchondral bone with risk for instability and disruption of adjacent articular cartilage that may result in premature osteoarthritis (12). The term osteochondritis dissecans was first coined by Konig in 1888, describing it as an inflammation of the bone-cartilage interface (16). Though it remains a well known condition, the cause is still unknown but trauma, ischaemia, defects in ossification and genetic causes have all been suggested (14). Classification of OCD can be based on age, location, radiographic and MRI findings, and intraoperative appearance. OCD is classified as a juvenile or adult form based on the skeletal maturity of the patiens (5). Juvenile OCD occurs in children and adolescents with open growth plates. Juvenile OCD has a much better prognosis than does adult OCD, with higher rates of spontaneous healing with nonoperative treatment (3). Although the majority of OCD lesions occur on the medial femoral condyle, they can occur anywhere.

Subchondral drilling for creation of revascularization channels is the primary surgical option used for treating juvenile OCD lesions. Standard drilling techniques either involve antegrade (transarticular) penetration of the intact articular cartilage or extra-articular (retrograde) approaches preserving the cartilage surface. The aim of this study is to review a total of 17 cases of juvenile OCD of the femoral condyle of the knee treated by transarticular drilling technique.

Materials and methods

The retrospective study included all patients with juvenile OCD operated between 2007 and 2014 in the orthopaedic department of our university hospital.

The records of all patients, between the age group of 5 to 17, diagnosed and surgically treated for juvenile OCD between 2007 and 2014 were reviewed. The following data were collected for each patient: demographics(age at diagnosis, gender), time between the conformation of diagnosis and operation, clinical finding, intensity of pain at admission graded from 0–10 according to the visual analog scale (VAS), plain radiograph films (antero-poterior and lateral views). All but two patients demonstrated radiographic evidence of juvenile OCD on plain radiographs, an MRI was carried out in the patients in whom radiographically the lesion was in early stages. There were a total of 8 boys and 9 girls with a mean age of 12.3 years. They were followed up for a mean period of 2.2 years. The average age at the time of surgery was 13.2 years. The mean time interval between the first clinical examination to the time of operation was 4.6 months and the mean duration of symptoms was 4.8 months. The affected knee, femoral condyles, preoperative Lysholm score, radiograph findings, arthroscopic

ACTA MEDICA (Hradec Králové) 2015; 58(3): 98–103
http://dx.doi.org/10.14712/18059694.2015.101

Tab. 1: Summary of patiens.

				Preoperative		Peroperative		Postoperative		
Patient	**Age**	**Knee**	**Location of lesion**	**Lysholm score**	**Radiographic grading**	**Arthroscopic grading**	**Size of lesion**	**Lysholm score**	**Radiographic grading**	**Treatment failure**
1	13	Left	MFC	88	III	II	**1 × 1 cm**	100	I	0
2	9.5	Right	LFC	88	III	II	**2 × 2 cm**	100	I	0
3	15	Left	MFC	81	III	II	**2 × 2 cm**	100	I	0
4	11	Right	LFC	81	II	II	**3 × 3 cm**	95	I	0
5	10	Right	MFC	81	II	II	**1 × 1 cm**	100	I	0
	10.5	Left	MFC	81	II	II	**1.5 × 1.5 cm**	100	I	0
6	13	Left	MFC	81	II	II	**1.5 × 1 cm**	95	I	0
7	15	Right	LFC	79	III	II	**2 × 3 cm**	95	I	0
8	11	Right	MFC	83	II	II	**2 × 1 cm**	100	I	0
9	15	Right	MFC	80	II	II	**1.5 × 1.5 cm**	100	I	0
10	15	Right	MFC	81	I	II	**2.5 × 1.5 cm**	100	I	0
11	12	Right	MFC	81	II	II	**1 × 1 cm**	100	I	0
	12.5	Left	MFC	81	II	II	**1.5 × 1.5 cm**	100	I	0
12	15	Right	MFC	79	III	II	**1.5 × 1 cm**	91	III	Unhealed (mosaicplasty)
13	15	Right	MFC	81	I	II	**2 × 2 cm**	95	I	0
	15	Right	LFC	81	I	II	**1.5 × 1.5 cm**	95	I	0
14	13	Right	LFC	81	III	II	**2.5 × 3 cm**	90	I	0
15	13	Left	MFC	83	III	II	**1.5 × 1.5 cm**	86	III	Unhealed (fixation)
	13.5	Right	MFC	83	III	II	**1 × 1 cm**	100	I	0
16	15	Right	MFC	81	III	II	**1 × 1 cm**	90	III	Unhealed (ACT)
17	15	Right	MFC	88	III	II	**1.5 × 1.5 cm**	83	III	Unhealed (ACT)

MFC – medial femoral condyle
LFC – lateral femoral condyle
ACT – autologous chondrocyte transplantation

Tab. 2: Grading of osteochondral lesions arthroscopically and radiographically.

Staging system for characterizing osteochondral lesions		
Grade	**Arthroscopic (Guhl)**	**Radiographs**
I	Irregularity and softening of articular Cartilage.No definable fragment	No findings
II	Articular cartilage breached, definable fragment, not displaceable	Subchondral radiolucency
III	Articular cartilage breached, definable fragment, Displaceable, but attached by some overlying articular cartilage	Well circumscribed area of subchondral bone separated by a sclerotic radiolucent outline of fragment
IV	Loose body	Loose body

findings and the postoperative Lysholm score and radiograph findings are detailed in Table 1.

On presentation a detailed physical examination was carried out which included range of movement of the knee joint, effusion of knee joint, quadriceps atrophy, presence of knee locking. The radiograph findings were graded from I to IV) (Table 2) (7).

All patients were advised non weight bearing of the affected side on crutches till the period of arthroscopy.

Arthroscopy had been taken under general or spinal anesthesia. No preventive antibiotics were administered during the operative procedure. Patients were operated with the use of a thigh tourniquet. Standard medial and lateral parapatellar portals were used. The articular cartilage was carefully visualized and probed to determine the extent of loosening at the site of lesion. The OCD lesion was then graded according to the classification by Guhl (9) (Table 2). All lesions were treated with transarticular drilling. For lesions of the lateral aspect of the medial femoral condyle, the medial portal is used as the viewing port and the lateral portal is used as the working portal and vice versa in lesions of the lateral femoral condyle. All lesions are drilled into the adjacent subchondral bone to a depth of 2 mm with a 1.2 mm smooth Kirschner wire to encourage bleeding at the base of the lesion and healing. The number of holes drilled depended on the size of the lesion(on an average between three and six). The number of holes drilled depended on the peroperative findings. What was more important, was that the holes were drilled 3 to 4 mm apart, while taking care not to damage the subchondral plate between the holes.

Postoperatively all patients were advised non weight bearing for a period of 6 weeks but immediate range of movement is allowed. Weight bearing was then gradually advanced but activities were still limited for a period of 3 months postoperatively. Sport activites were permitted after a period of 6 months.

Postoperative Evaluation

Postoperative evaluation included clinical and radiographic examination at follow-up visits to monitor healing. Radiographs included AP, lateral views. In one case an MRI and in another case a CT was carried out to determine extent of healing. Healing on radiographs was defined as disappearance of the radiolucent zone or union of the displaced fragment. We used the Lysholm score to assess improvement in knee function. In addition, clinical improvement in symptoms was measured using VAS.

Results

Out of the 17 patients, 7 players were involved in active sporting activities like football or judo, interestingly 3 patients with lateral femoral condyle lesions had previously undergone arthroscopy of the knee for modellation of lateral discoid meniscus, 1 patient had habitual subluxation of patella, and the remaining were not involved in any sporting activities. The most common complaint was poorely localised knee pain, no patient presented with knee effusion, quadriceps atrophy.

OCD was diagnosed in 19 of the 21 knees from plain X-ray films alone, while in the remaining two knees an MRI was carried out in the patients in whom radiographically the lesion was in early stages. We classified the lesions radiographically as well as arthroscopically accorging to Guhl (9) (Table 2). Interestingly, one patient had OCD of both the femoral condyles of the right knee.

Postoperatively, there was an overall improvement in Lysholm knee score from a mean preoperative score of 82.2 to a mean postoperative score of 96. Radiographically, 17 of grade III or grade II lesions improved to grade I lesion, while the remaining four grade III lesions remained stationary and had to undergo further procedures. In four patients despite showing no radiographic signs of improvement, there was an improvement in VAS and Lysholm scores.

The visual analog score was used to measure the subjective improvement in symptoms. There was a significant decrease in VAS pre and postoperatively from 5.45 to 1.55. No post-operative infection or thromboflebitis occured. The only complication that was encountered were unhealed lesions following transarticular drilling. In our study one patient had to undergo mosaicplasty, 2 patients had to ACT, while one patient had to undergo fixation of the fragment with the help of Herbert screws for no radiographic signs of

Fig. 1:
Pre-operative AP view of the knee showing an OCD lesion (black arrows).

Fig. 2:
Post-operative AP view of the knee 5 months after transarticular drilling demonstrating completely healed OCD lesion.

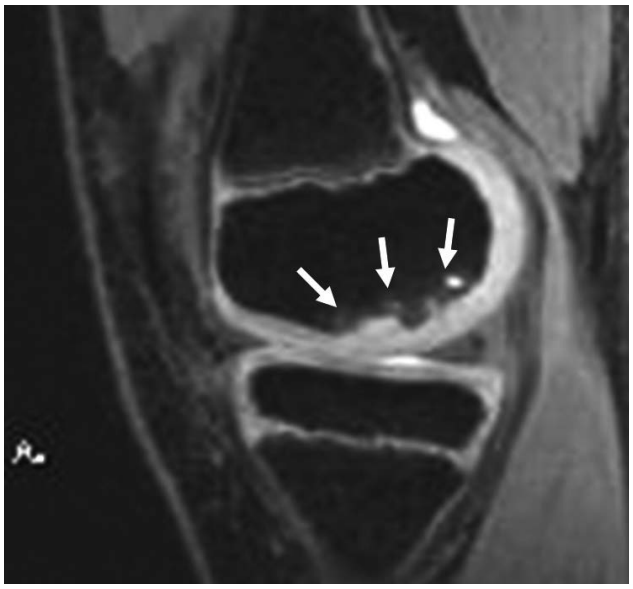

Fig. 3: MRI – sagittal section showing OCD lesion (white arrows).

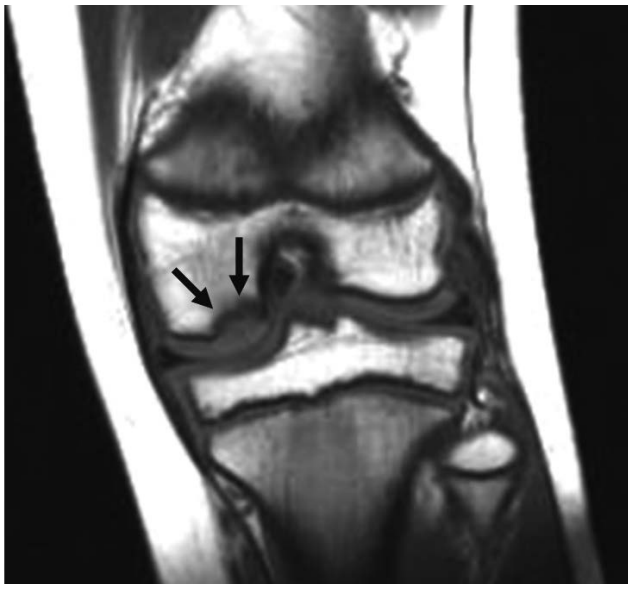

Fig. 4: MRI – frontal section showing OCD lesion (black arrows).

healing. All these patients after the above mentioned operations had satisfactory results.

Discussion

OCD is a localized condition of subchondral bone and overlying cartilage most commonly occuring in the knee. Possible causative factors of OCD include repetitive microtrauma, ischemia, genetic and endocrine factors and anomalies of ossification (16). A multicenter study carried out by the European Pediatric Orthopaedic Society showed that nearly 55% of the patients with OCD were either regularly active in sports or performed strenous athletic activity (11). OCD most commonly affects the medial femoral condyle, rarely the lateral femoral condyle is affected. Interestingly, in our study one patient had OCD lesion of both the femoral condyles. Hanna et al. (10) also reported two cases of bicondylar OCD of the knee. Prior to their study no case of bicondylar OCD of the knee had been reported. Furthermore, the presence of discoid meniscus has also been reported to play a role in the development of OCD. Discoid menisci are abnormal in macroscopic and microscopic struc-

ture. Their ability to provide normal articular surface and subchondral region load sharing and stress shielding has not been documented. Alterations of joint mechanics produced by a tear of the discoid meniscus with fragment instability and compromised joint function may produce increases in peak loading forces such as those documented following compromise of menisci of normal morphology. This modification may allow repetitive micro-trauma to summate in forces that produce a subchondral lesion.

Treatment of OCD depends on age of presentation, fragment size, fragment location and fragment stability. Stable lesions in skeletally immature patients are more amenable to conservative management (19). The disruption of subchondral blood supply is an important factor in the development of OCD (20). Fragment healing is enhanced by creating vascular channels to the devitalized region, also known as drilling. Today arthroscopic or open drilling, either alone or with various fixation methods, remains one of the most common operative interventions. Open drilling and reduction was first proposed by Smillie in 1957 (18), since then many authors have suggested drilling alone or with various fixation methods and it still remains the most common operative procedure for OCD lesions. Multiple authors have reported high rates of healing with arthroscopic drilling. Kocher et al. (13) reported 100% radiographic healing in 30 skeletally immature knees treated with transarticular arthroscopic drilling after an average of 4.4 months, and Aglietti et al. (1) and Bradley and Dandy (4) reported 95% and 82% radiographic healing, respectively.

An alternative method is retrograde drilling, which does not violate the intact articular cartilage. However, retrograde drilling is a technically demanding operation that requires fluoroscopy (2).

Irrespective of the drilling technique used, drilling still remains an effective treatment option for stable OCD lesions, especially in patients with open physes who tend to have greater healing potential.

A variety of treatments have evolved over the past few years aimed at addressing irreparable chondral defects and OCD lesions. These include microfracture, autologous chondrocyte transplantation, mosaicplasty. These techniques are reserved for unsalvageble lesions such as those with extensive comminution, fragmentation or with chronic complete detachent of the chondral lesion. Newer surgical treatments, including single-stage cell-based procedures, use mesenchymal stem cells and matrix augmentation (8).

The treatment of osteochondral lesions in the knee is dictated by the stability of the osteochondral fragment and thus the overlying cartilage. Though standard anteroposterior and lateral radiographs of the knee permit localalization of the lesion, they however do not permit visualization of the articular cartilage and do not indicate whether there is fibrous attachment of the osteochondral fragment to the underlying bone. Furthermore, most the the times it is difficult to distinguish between grade II and grade III lesions on plain radiograph films.

Recent studies have advocated the use of MRI as an accurate method of preoperative staging for osteochondral lesions. A classification system has been devised by Dipaola et al. (6) to stage OCD on MRI (Table 3).

The most useful diagnostic feature of MRI is the ability to distinguish between Stage II and Stage III lesion. In Stage II lesion with stable fibrous attachment, a heterogenous area of mixed higher and lower signal intensity is seen behind the lesion. In contrast, Stage III lesions will show a thin, homogenus intermediate signal behind the lesion, indicating synovial fluid between the fragment and underlying subchondral bone. The ability to distinguish between Stage II and Stage III lesions preoperatively is useful in planning surgery. Stage II lesions are stable and have mostly intact articular cartilage, which can be treated by drilling for revascularisation of the fragment. Stage III lesions are unstable and require fixation in addition to drilling to maximize chances of healing.

A recent study by O'Connor et al. (15) has further improved the accuracy of MRI staging the OCD lesion from 45% to 85% by interpretating the high signal T2 line as a predictor of instability only when it was accompanied by a breach in the cartilage on the T1-weighted image. According to this study the appearance of a high signal line on T2-weighted image does not mean a poor prognosis for the lesion. This high signal line may represent vascular granulation tissue and hence a healing response. Only if this high signal line is associated with a break in the articular cartilage, seen on T1-weighted image, it can be said to represent synovial fluid. If there is no such breach the lesion can be treated conservatively since healing may occur without surgery.

Currently, MRI is the preferred imaging modality for both diagnosis and the assessment of healing potential of OCD of the knee due to its ability to provide excellent anatomical detail of both the bone and soft tissue structures with the absence of harmful ionizing radiation (17).

Tab. 3: Classification of OCD lesions on MRI.

Staging system for characterizing osteochondral lesions	
Stage I	Thickening of articular cartilage and low signal changes
Stage II	Articular cartilage breached, low signal rim behind fragment indicating fibrous attachment
Stage III	Articular cartilage breached, high signal changes behind fragment indicating synovial fluid between fragment and underlying subchondral bone
Stage IV	Loose body

Conclusion

In conclusion OCD of the knee should be considered to a differential diagnosis among children with acute or subactue knee pain. The history, physical examination, imaging examinations (especially MRI) and arthroscopy are important for the early diagnosis and conservative or surgical management of the process aimed at preserving the cartilage and joint congruence. Untreated or inadequately treated lesions may progress from stable, intact lesions to unstable lesions with loose body formation, chondral tears, and full thickness defects with underlying loose fibrous tissue. Allowing these patients to continue their acitivities unchanged despite intermittent pain, mechanical symptoms and radiographic changes is to allow patient to potentially progress to significant early gonarthrosis. Reestablishment of the joint surface, improvement of the fragment's blood supply, rigid fixation, and early motion are the primary goals for osteochondral fragment preservation. When the fragement is not suitable for preservation, careful consideration of defect location and the patient's clinical presentation will determine when cartilage restoration procedures should be performed. Successful restorative options should relieve pain, restore function and prevent the development of secondary gonarthrosis.

For the future, based on the retrospective study of our pateints with JOCD lesions we have come to two main concluions. Firstly, every patient diagnosed with OCD must undergo MRI, to enable proper preoperative staging of OCD lesions and then depending on the grade of lesion, plan proper treatment. Secondly, all grade I or grade II lesions, can be treated conservatively for a minimum period of six months after which a control MRI should be cariried out. In our study we were not able to differentiate between grade II and grade III lesions on X-rays which lead to unfavourable results in two cases, we therefore recommend preoperative MRI of every OCD lesion for proper grading of the lesion and subsequent planning of treatment. If there are no signs of healing or if the lesion is unstable, then the lesion is ought to be treated surgically, either just drilling or fixation in addition to drilling to maximize the chances of healing.

Acknowledgements

This work was supported by the programme PRVOUK P37/04 and by MHCZ-DRO (UHHK, 00179906).

References

1 Agletti P, Buzzi R, Bassi PB, et al. Arthroscopic drilling in juvenile osteochondritis of the medial femoral condyle. Arthroscopy 1994; 10: 286–291.

2. Boughanem J, Riaz R, Patel RM, Sarwark JF. Functional and radiographic outcomes of juvenile osteochondritis dissecans of the knee treated with extra-articular retrograde drilling Am J Sports Med 2011; 39(10): 2212–7.
3. Bradley J, Dandy DJ. Osteochondritis dissecans and other lesions of the femoral condyles. J Bone Joint Surgery Br 1989; 71(3): 518–522.
4. Bradley J, Dandy DJ. Results of drilling osteochondritis dissecans before skeletal maturity. J Bone Joint Surgery Br 1989; 71: 642–644.
5. Cahill BR. Osteochondritis dissecans of the knee: treatment of juvenile and adult forms. J Am Acad Orthop Surg 1995; 3(4): 237–247.
6. Dipaola J, Nelson DN, Colville MR. Charecterising osteochonral lesions by magnetic resonance imaging. Arthroscopy 1991; 7: 101–104.
7. Book: Dungl P et al. (2005) Ortopedie. Prague, Grada publishing.
8. Erickson BJ, Chambers PN, Yanke AB, et al. Surgical management of osteochondritis dissecans of the knee. Curr Rev Musculoskelet Med 2013; 6: 102–114.
9. Guhl JF. Arthroscopic treatment of osteochondritis dissecans. Clin Orthop 1982; 167: 65–74.
10. Hanna SA, Aston WJS, Gikas PD, Briggs TWR. Bicondylar osteochondritis dissecans in the knee. J Bone Joint Surg Br 2008; 90-B: 232–235.
11. Hefti F, Beguiristain J, Krauspe R, et al. Osteochondritis dissecans, a multicenter study of the European Pediatric Orthopedic Society. J Pediatr Orthop B 1999; 8: 231–245.
12. Chambers HG, Shea KG, Anderson AF, et al. American Academy of Orthopaedic Surgeons Clinical Practise Guideline on: The diagnosis and Treatment of Osteochondritis Dissecans. J Bone Joint Surg Am 2012; 94(14): 1322–1324.
13. Kocher MS, Micheli LJ, Yaniv M, et al. Functional and radiographic outcome of juvenile osteochondritis of the knee treated with transarticular arthroscopic drilling. Am J Sports med 2001; 29(5): 562–566.
14. Kocher MS, Tucker R, Ganley TJ, Flynn JM. Management of Osteochondritis dissecans of the knee. Current concepts review. Am J Sports Med 2006; 34(8): 1181–1191.
15. O'Connor MA, Palaniappan M, Khan N, et al. Osteochondritis dissecans of the knee in children. A comparison of MRI and arthroscopic findings. J Bone Joint Surg Br 2002; 84: 258–262.
16. Scenck R, Goodnight JM. Osteochondritis dissecans. J Bone Joint Surg 1996; 78: 439–456.
17. Schultz JF, Chambers HG. Juvenile osteochondritis of the knee. Current concepts in diagnosis and management. Instr Course Lect 2013; 62: 455–467.
18. Smillie IS. Treatment of osteochondritis dissecans. J Bone Joint Surg Br 1957; 39: 248–260.
19. Wall E, Von Stein D. Juvenile osteochondritis dissecans. Orthop Clin North Am 2003; 34: 341–353.
20. Williams JS Jr, Bush-Joseph CA, Bach Br Jr. Osteochondritis dissecans of the knee. Am J Knee Surg 1998; 11: 221–232.

Received: 16/04/2015
Accepted in revised form: 09/09/2015

Corresponding author:

Haroun Hassan Shaikh, Department of Orthopedic Surgery, Teaching Hospital in Hradec Králové, Sokolská 581, Hradec Králové, Czech Republic; e-mail: haroun.shaikh@fnhk.cz

SHORT COMMUNICATION

NEEDS OF HOSPITALIZED SCHIZOPHRENIC PATIENTS IN THE NORTH MORAVIA AND THE CZECH PART OF SILESIA

***Jiřina Hosáková*[1], *Ladislav Hosák*[2]**

Institute of Nursing, Faculty of Public Policies, Silesian University in Opava, Czech Republic[1]; Department of Psychiatry, Charles University in Prague, Faculty of Medicine in Hradec Králové and University Hospital Hradec Králové, Czech Republic[2]

Summary: Objectives: The main aim of the study was to investigate the physiological and social needs of patients hospitalized with schizophrenia to uncover potential issues in these areas. Methods: The relevant self-evaluating CANSAS questionnaire for physiological and social needs was used by nurses in a cohort of hospitalized schizophrenic patients undergoing rehabilitation before discharge from the mental hospital. Results: Two hundred and forty-four patients (women N = 115) aged 18–58 years were involved in the study. Intimate relations, financial matters, treatment of psychotic symptoms, and sexual life were among the most pressing physiological and social needs in our study subjects. Conclusion: The results of our study should stimulate psychiatric nurses in their effort not only to detect but also address the problems of schizophrenic patients concerning unfulfilled needs.

Keywords: *Schizophrenia; Physiological and Social Needs; Psychiatric Nursing; Mental Health Care Reform*

Introduction

Schizophrenia is one of the most serious mental disorders. It affects around 0.3–0.7% of people at some point in their life (4). Delusions, hallucinations, disorganized thinking, abnormal motor behavior, negative symptoms and cognitive deficit are among the most striking symptoms of schizophrenia. These psychopathological phenomena impair the patients' ability to act comprehensibly, function in social relationships, find and maintain a paid job, and live up to natural expectations (8).

According to Maslow's hierarchy of needs, physiological needs of a human being represent a physiological call of nature which must be met for the subject to live and for his or her health status not to be endangered (3). Social needs are among the so-called "higher needs" and comprise the needs for social contact and support, love, and social self-assertion. The physiological as well as social needs of people suffering from schizophrenia are typically under-accomplished (4).

The purpose of the study was to assess the physiological and social needs of hospitalized schizophrenia patients. This has recently become a "hot" topic in the Czech Republic due to planned mental health care reform. The reform seeks intensive expansion of extramural psychiatric services and extensive involvement of psychiatric nurses in the treatment and rehabilitation of people with serious mental disorders, including schizophrenia (7).

Subjects and Methods

Subjects

Hospitalized patients suffering from schizophrenia at the Mental Hospital Opava, Czech Republic from the period of September 2011–June 2014 were asked to participate. The North Moravia and the Czech part of Silesia are the catchment area of this large psychiatric institution. The following inclusion criteria were applied: Age 18–65 years, diagnosis of schizophrenia (F20 according to the ICD-10 classification), voluntary treatment in the hospital, and a willingness to participate in the research. The patients were hospitalized at an open ward mostly aimed at rehabilitation and resocialization. They had already undergone acute pharmacological treatment for schizophrenic episode at a locked psychiatric ward several weeks prior.

We did not examine healthy volunteers because the previous research employing the assessment method of quality of life and needs of the study subjects had already been carried out in the Czech Republic, and the literature allowed us ample access to data concerning the results (2).

Methods

Sociodemographic data on the study's participants (age, gender, education, occupation, family status and number of

ACTA MEDICA (Hradec Králové) 2015; 58(3): 104–107
http://dx.doi.org/10.14712/18059694.2015.102

psychiatric hospitalizations in the patient's life) were obtained from medical records.

We used the Camberwell Assessment of Need questionnaire – the short version (CANSAS) – for every study subject. This tool is intended to survey the physiological and social needs of mentally ill individuals, i.e. whether the needs are met or not. CANSAS includes 22 items related to housing conditions, daily activities, physical health, mental problems, threats to the patient or other people, substance abuse, friends, sexuality, care of children, education, transportation, or finances. Each item is assessed by the responder as to whether this need is satisfied or not (non-existent need/no serious problem = 0 points; the need has recently been addressed with the help of professional caretakers = 1 point; the need has not been fulfilled = 2 points). This means that for items with 1 or 2 points, professional help should be continued (1 point) or applied anew (2 points). The Camberwell Assessment of Need was first introduced in 1995 and is described in detail elsewhere (5). A Czech version of CANSAS has also been validated (6).

The CANSAS questionnaire was applied and its significance was explained to the patients by psychiatric nurses, participating in the research.

Statistics

We used the two-sample Student's t-test. If individual parameters were analyzed (age, employment status, living with a partner), we applied the non-parametric Wilcoxon test and Kruskal-Wallis test. A result was considered statistically significant if $p < 0.05$. We used the Stata v. 13 statistical program.

Ethical issues

The work was approved by the Ethics Committee, Faculty of Medicine, University of Ostrava, Czech Republic on the 20th of June, 2011 (EK 3/2011). The subjects voluntarily gave their informed consent to participate. The study was performed in accordance with the principles of the Declaration of Helsinki of 1975, as revised in 2000.

Results

Sociodemographic data on the study sample

The total number of schizophrenia patients included into the study was 244 (women N = 115). Sociodemographic data on the study sample are stated in detail in Table 1.

To sum up, a typical participant was a male aged 18–29, living in a city of 10,000–50,000 inhabitants, with a high-school education, receiving a disability pension, with an "average" economic background, single, childless, and recently hospitalized at a psychiatric ward for the 2nd–3rd time in his life.

Tab. 1: Sociodemographic data on the study sample of schizophrenia patients (N = 244; women N = 115).

Variable	Proportion of the study sample (%)
Age range (years)	
18–29	52
30–44	37
45–58	11
Residence (inhabitants)	
Less than 10,000	24
10,000–50,000	37
50,000–100,000	22
100,000 and more	17
Education	
Primary school	8
Vocational school	36
High school	46
University	10
Employment	
Disability pension	42
Unemployed	25
Employed	13
Student	11
Retiree	4
Entrepreneur	2
Maternity leave	1
Housewife	1
Not stated	1
The current financial situation	
Substantially above-average	1
Moderately above-average	5
Average	41
Moderately below-average	38
Substanitally below-average	15
Marital status	
Single	59
Married or a similar relationship	27
Divorced	14
Children	
No	70
Yes	30
Order of the current psychiatric hospitalization	
1st	30
2nd–3rd	34
4th–5th	19
6th or further	17

Physiological and social needs of the patients

According to the CANSAS questionnaire results, intimate relations, financial situation and treatment of psychotic symptoms were among the most unfulfilled items in general, while in the subgroup of men sexual life was also stated ($p = 0.016$; two-sample Student's t-test). This was not influ-

enced by age or employment status (p = NS; Wilcoxon test, Kruskal-Wallis test). On the other hand, patients living with a partner more often perceived their physiological and social needs to be met in comparison with study subjects who were single ($p < 0.05$; Wilcoxon test). The CANSAS results of schizophrenia patients are shown in Table 2.

Tab. 2: The Camberwell Assessment of Need questionnaire (CANSAS) – results in 244 patients with schizophrenia.

Item	Arithm. mean	Sd
Housing	0.16	0.36
Nourishment	0.08	0.28
Housekeeping	0.11	0.32
Self-care	0.06	0.25
Daily activities	0.28	0.66
Physical health	0.22	0.41
Psychotic symptoms	1.06	0.98
Informations on health	0.23	0.42
Mental problems	0.72	0.55
Threat to oneself	0.40	0.49
Threat to others	0.34	0.86
Alcohol	0.19	0.39
Illegal drugs	0.21	0.41
Friends	0.46	0.84
Intimate relationships	0.96	1.10
Sexuality	0.93	1.09
Care of children	0.24	0.43
Education	0.08	0.28
Telephoning	0.04	0.21
Transportation	0.30	0.67
Finances	0.51	0.79
Financial benefits	1.00	2.13

Discussion

Our patients mostly indicated that their unmet physiological and social needs involved social relations, finances, treatment of psychotic symptoms, and sexual life, all of which is understandable. As stated above in the sociodemographic data section, a typical respondent in the study was a single male, receiving a disability pension, and hospitalized for schizophrenia. Our results are similar to the ones ascertained by Wennstrom et al. (9). The authors investigated 741 outpatients with schizophrenia and other psychotic disorders in Sweden. The main difference in the Wennstrom's study sample was that finances were not seen as such a pressing issue as in our study. This may be due to mentally ill people in Sweden being in better position financially than those in the Czech Republic.

Our study also concurred with Brain et al. (1) in revealing the importance of close social relationships in the lives of schizophrenic patients. The authors studied 111 outpatients with schizophrenia and schizophrenia-like psychosis. If the study subjects felt stigmatized and discriminated against, social relationships (including intimate ones) were perceived as the most important domain. On the other hand, a quality partnership may help the patient to overcome his or her troubles better.

The subjective assessment of needs as well as the use of the CANSAS questionnaire only for hospitalized schizophrenic patients represents the limitations of our study. A more comprehensive view would be obtained if objective tools were utilized not only in inpatients but also on an outpatient basis. This attitude may be employed in future research.

The patients suffering from schizophrenia and this mental disorder itself are specific, different from other mental disorders (for example major depression, anxiety disorders) or physical diseases. A lack of insight in schizophrenia is typical, which may distort the subjective evaluation of psychotic symptoms or feeling of the disease in general. This should be taken into consideration in the interpretation of the study results.

On the other hand, a relatively large and homogenous study sample is one of the strong points of our research.

Conclusions

The practical outcome of our study can be to stimulate psychiatric nurses in their effort to continuously detect and take care of problems concerning the unmet needs of patients with schizophrenia. Further research in this field could be performed by monitoring the needs of schizophrenic patients before and after the systematic education by psychiatric nurses and optimization of nursing care. This is especially important in the Czech Republic, where legislative reform of mental health care emphasizing community care and psychiatric nursing has recently been implemented.

References

1. Brain C, Sameby B, Allerby K, et al. Stigma, discrimination and medication adherence in schizophrenia: results from the Swedish COAST study. Psychiat Res 2014; 220: 811–7.
2. Dragomirecka E, Bartonova J, Motlova L, et al. SQUALA. Prirucka pro uzivatele české verze Dotazniku subjektivni kvality zivota SQUALA. 1st ed. Prague: Psychiatric Center Prague, 2006: 68.
3. Maslow AH, Abraham H. A Theory of Human Motivation. Psychol Rev 1943; 50: 370–6.
4. van Os J, Kapur S. Schizophrenia. Lancet 2009; 374: 635–45.

5. Phelan M, Slade M, Thornicroft G, et al. The Camberwell Assessment of Need: the validity and reliability of an instrument to assess the needs of people with severe mental illness. Br J Psychiat 1995; 167: 589–95.
6. Probstova V, Selepova P, Dragomirecka E, et al. Pece o dusevni zdravi. Metody hodnoceni. CAN: Camberwellske setreni potreb. 1st ed. Prague: Centrum pro rozvoj pece o dusevni zdravi, 2006: 63.
7. Tresnak P. Taking mental health into the community. Bull World Health Organ 2014; 92: 702–3.
8. Weinberger DR, Harrison P. Schizophrenia. 3rd ed. Oxford: Wiley-Blackwell, 2011: 722.
9. Wennstrom E, Sorbom D, Wiesel FA. Factor structure in the Camberwell Assessment of Need. Br J Psychiat 2004; 185: 505–10.

Received: 02/07/2015
Accepted in revised form: 26/08/2015

Corresponding author:

Jiřina Hosáková, MSc., The Institute of Nursing, Hauerova 4, 746 01 Opava, Czech Republic; e-mail: jirina.hosakova@fvp.slu.cz

ENCEPHALITIS WITH PROLONGED BUT REVERSIBLE SPLENIAL LESION

Alena Meleková[1], *Leona Andrlová*[1], *Pavel Král*[2], *Leoš Ungermann*[2], *Edvard Ehler*[1]

Department of Neurology, Hospital of the Pardubice Region, and Faculty of Health Studies, University of Pardubice, Czech Republic[1]; Department of Radiology, Hospital of the Pardubice Region, and Faculty of Health Studies, University of Pardubice[2]

Summary: Introduction: The splenium of the corpus callosum has a specific structure of blood supply with a tendency towards blood-brain barrier breakdown, intramyelinic edema, and damage due to hypoxia or toxins. Signs and symptoms of reversible syndrome of the splenium of the corpus callosum typically include disorientation, confusion, impaired consciousness, and epileptic seizures. Case report: A previously healthy 32-year-old man suffered from weakness, headache, and fever. Subsequently, he developed apathy, ataxia, and inability to walk, and therefore was admitted to the hospital. Cerebrospinal fluid showed protein elevation (0.9 g/l) and pleocytosis (232/1 ul). A brain MRI showed hyperintense lesions in the middle of the corpus callosum. The patient was treated with antibiotics, and subsequently, in combination with steroids. Two months later, the hyperintense lesions in the splenium and the basal ganglia had disappeared. Almost seven months since his hospitalization in the Department of Neurology, the patient has returned to his previous employment. He now does not exhibit any mental changes, an optic edema and urological problems have improved. In addition, he is now actively engaged in sports. Conclusion: We have described a case of a 32-year-old man with confusion, ataxia, and inability to stand and walk. The man developed a febrile meningeal syndrome and a hyperintense lesion of the splenium, which lasted for two months. Neurological changes, optic nerve edema, and urinary retention have resolved over the course of seven months. We think that the prolonged but transient lesion of the splenium may have been caused by encephalitis of viral origin.

Keywords: *Splenium of the corpus callosum; T2-weighted lesion; Optic nerve edema; Confusion; Encephalitis*

Introduction

Corpus callosum is the largest commissural pathway consisting of myelinated axons that cross the midline and connect homologous regions of both hemispheres. Magnetic resonance imaging (MRI) may commonly and unexpectedly display abnormalities of the splenium of the corpus callosum (SCC). Typically, such SCC lesions are reversible and are associated with various clinical symptoms (confusion, delirium, epileptic seizures) and etiologies (ischemic infarction, trauma, tumors, alcohol abuse, intoxication, and hypopituitarism) (7). Numerous studies have been conducted and case reports have been published; nonetheless, the body of knowledge concerning the SCC remains sketchy (2). A reversible lesion with transiently reduced diffusion in the SCC has been reported in patients with clinically mild encephalitis/encephalopathy, leading to a new clinical-radiological syndrome – mild encephalitis/encephalopathy with a reversible splenial lesion (MERS). Lesions in the middle of the SCC or MERS have been described in various infectious diseases (herpes, rickettsia, and influenza) and also after vaccination (11). We describe a case of a previously healthy man, who presented with a two-week history of fever and who developed meningeal syndrome, confusion, urinary retention, and other, mild signs of brain dysfunction. An MRI scan revealed hyperintense lesions in the middle of the SCC, lasting for more than two months.

Case report

A previously healthy 32-year-old man suffered from flu-like symptoms in July 2014 along with fever and weakness. He was treated by antibiotics and recovered. His condition improved for three weeks. Subsequently, the patient developed a fever, headache, a generalized body ache, and psychomotor decline. He was admitted to the urology department of a regional hospital with urinary retention and was treated with antibiotics (trimethoprim + sulfamethoxazole) for suspected urinary infection.

As the patient's condition was not improving, he was examined by a neurologist. A lumbar puncture was performed, and proteinocytologic dissociation was found: proteins

ACTA MEDICA (Hradec Králové) 2015; 58(3): 108–112
http://dx.doi.org/10.14712/18059694.2015.103

1.2 g/l (0.20–0.40); leukocytes 3.7 × 10^6/l (0.0–5.0); glucose 2.4 mmol/l (2.50–4.50); lactate 2.9 mmol/l (1.20–2.10). With suspected meningoencephalitis he was transferred to our hospital, Department of Infectious Diseases. The patient's condition deteriorated rapidly. The examination revealed meningeal and cerebellar syndrome and another lumbal puncture (LP) was performed with a corresponding finding: a protein level of 0.9 g/l; a leukocyte count 232.0 × 10^6/l, only 3 days after the first lumbal puncture! He was treated by acyclovir and ceftriaxone. A brain MRI was performed, which showed T2 hyperintense lesions in the central part of the splenium of the corpus callosum. Similar, smaller lesions were identified in the area of the left thalamus, the basal ganglia, and the brainstem.

Since the patient's condition was not improving, he was transferred to the Neurological Intensive Care Unit (ICU). His neurological examination revealed cognitive and behavioral deficiency, meningeal syndrome, and minor multifocal symptoms originating in the right hemisphere, the cerebellum, and the extrapyramidal system. Urological examination showed persistent urinary retention, and ophthalmic examination led to the diagnosis of papillary congestion.

The patient was hospitalized in the Department of Neurology for a total of two months. A total of seven LPs were performed. Most of them to relieve the fluid pressure. The cytologic findings of the cerebrospinal fluid (CSF) revealed uniform population of lymphocytes but the immune phenotyping was normal, so the lymphoma was not proved. The laboratory findings of the CSF gradually improved: in a week – proteins 0.88 g/l; leukocytes 209.0 × 10^6/l, in two weeks – proteins 0.51 g/l; leukocytes 116.0 × 10^6/l. And so the CSF opening pressure, from 575 mm H_2O to 425 mm H_2O (200–300 mm H_2O) with a patient sitting up. The last CSF finding was: proteins 0.4 g/l; leukocytes 36.0 × 10^6/l.

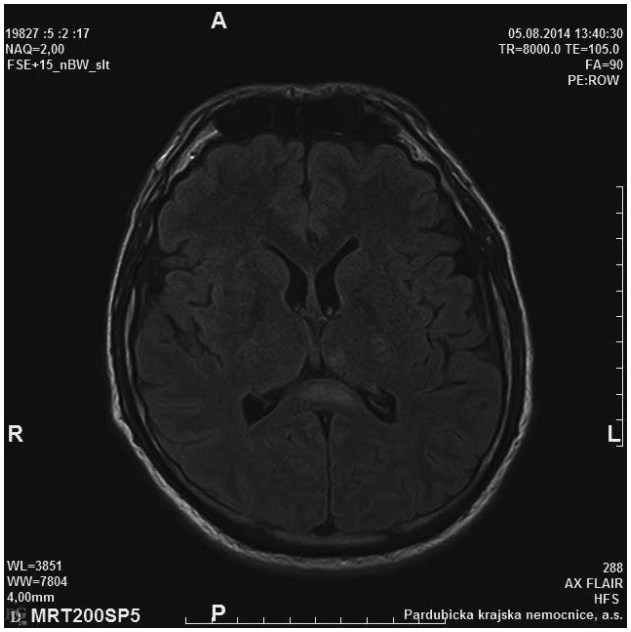

Fig. 1: MRI of the brain, axial FLAIR – hyperintense lesions of the splenium of the corpus callosum and the left thalamus.

A repeat MRI scan of the brain, performed approximately one month later, showed regression of the most extensive lesion in the splenium of the corpus callosum and also of the minor multifocal lesions in the basal ganglia and the thalamus bilaterally. Two months later, complete regression was present.

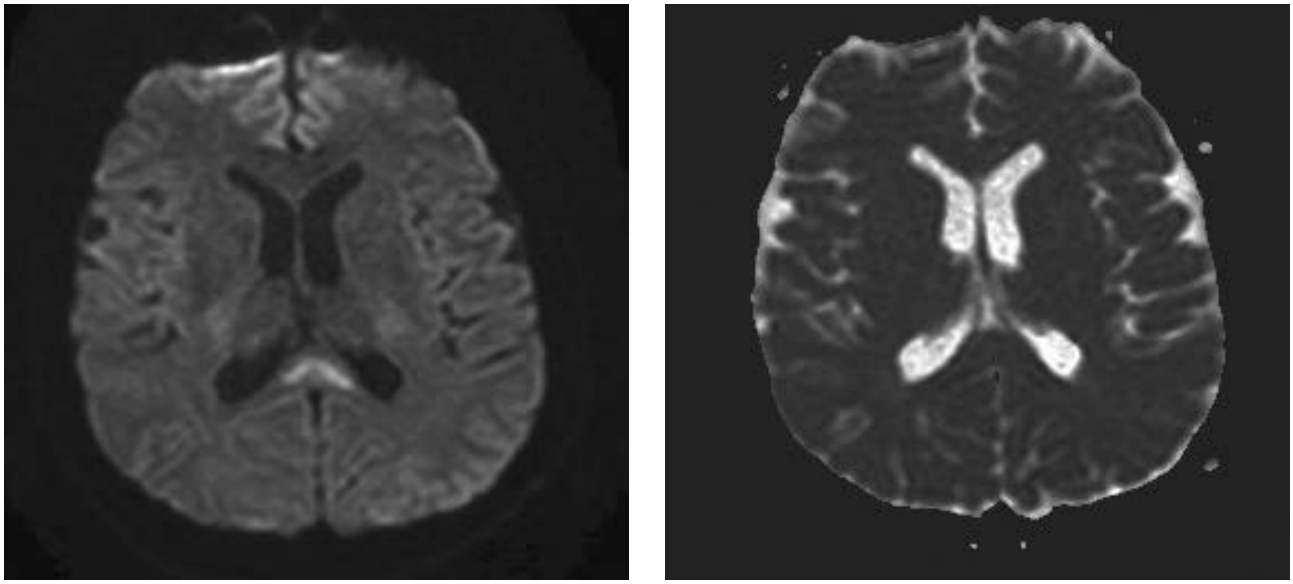

Fig. 2: MRI of the brain, ADC/DWI – hyperintense lesions of the splenium of the corpus callosum: a) MRI of the brain, DWI; b) MRI of the brain, ADC.

Treatment of the patient proved to be very difficult. The origin of the meningoencephalitis was not found. The patient was treated with acyclovir and ceftriaxone. After three weeks, the patient was started on meropenem. Subsequently, methylprednisolone pulse therapy (a total amount of 3 grams) was given for a period of 11 days.

Urinary retention was present during almost the entire hospitalization period; therefore, an indwelling urinary catheter was used. Furthermore, the patient was treated with tamsulosin and distigmine bromide and was followed-up in an outpatient clinic in regular intervals over a period of six months. Nowadays he is treated only with tamsulosine.

In the Ophthalmology Department, regular follow-up assessments of the papillary congestion were performed, using optical coherence tomography (OCT). The patient was taking acetazolamide and the papillary edema had regressed after the period of six months.

The patient's neurological examinations have revealed continuing improvement of his condition. Gradual verticalization was started, first using a stand tall walker, and later the forearm crutches. Finally, the patient's gait became stable even without any assistive aids.

The patient was unfit for work for a total period of seven months. Nowadays, the patient is without any subjective problems. He is feeling well, and has started doing sports – running. The patient's memory and cognitive function have returned to baseline.

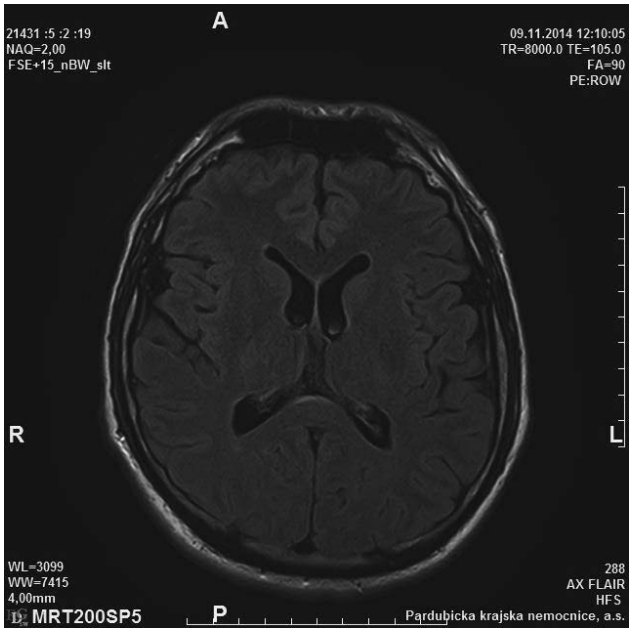

Fig. 3: MRI of the brain, axial FLAIR – total regression of hyperintense lesions.

Discussion

We have described a case of a 32-year-old man with confusion, meningeal syndrome, and a hyperintense lesion on MRI (T2-weighted images) in the middle of the corpus callosum. This is unique due to the duration of the T2 lesion (a period of 2 months) and the associated urinary retention and edema of the optic nerve, which completely resolved over a period of seven months. In our patient, we think that the reversible SCC lesion was caused by viral encephalitis. The laboratory findings did not detect any autoimmune parainfectious process.

The corpus callosum is the largest commissural pathway consisting of the cross-sectional area representing twice the magnitude of the sum of all other commissural structures

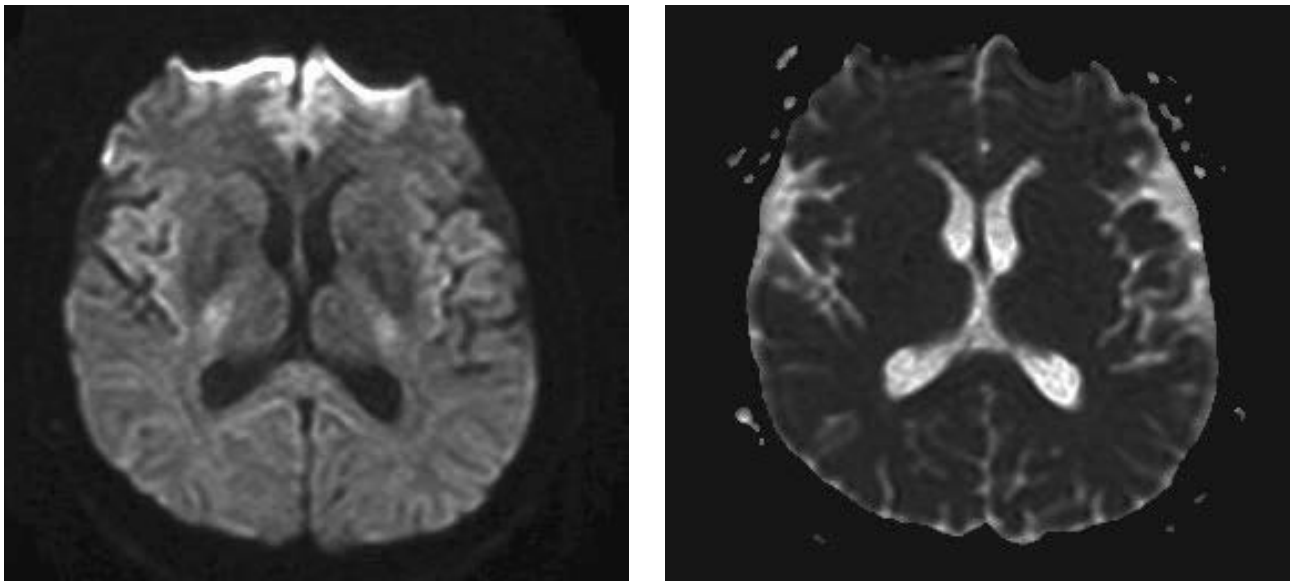

Fig. 4: MRI of the brain, ADC/DWI – total regression of hyperintense lesions: a) MRI of the brain, DWI; b) MRI of the brain, ADC.

in the brain of an adult. It consists of myelinated axons that cross the midline in the developing brain in order to connect homologous regions of both hemispheres (5). The splenium receives its arterial supply from the vertebrobasilar system. The exact mechanism of the development of transient splenial hyperintensity is not known. Some of the proposed mechanisms are blood-brain barrier breakdown, intramyelinic edema due to inflammation and migration of inflammatory cells, extrapontine osmotic myelinolysis due to sodium and glucose imbalance, and direct viral invasion or hypersensitivity to antiepileptic drugs. Studies about post-traumatic lesions in the corpus callosum generally explain the prevalence of callosal injury by its vulnerability to shearing forces (8). In our patient, we presume the presence of an inflammatory mechanism, with intramyelinic edema lasting for more than one month.

Clinical manifestations of reversible syndrome of the splenium of the corpus callosum include disorientation, confusion, epileptic seizures, headache, ataxia, symptoms of hemispheric disconnection, dysarthria, hallucinations, and impaired consciousness progressing to coma (2). Confusion was the most common clinical finding in 50% of cases. Cerebral infarction was the most common etiology (50%). The most consistent SCC changes on MRI were low signal on T1WI (T1-weighted images), high signal on T2WI and FLAIR, and high signal on DWI. SCC lesions are classified into in situ SCC lesions (SCC only) and multiple (SCC plus) lesions for patients with multiple lesions (7). In our patient, the T2 hyperintense lesion was in the middle of the SCC; furthermore, a small lesion was present in the left thalamus.

Shankar et al. presented a case of mild encephalitis with a reversible splenial lesion (MERS), evaluated with diffusion-weighted and diffusion tensor imaging along with various conventional sequences of MRI (10). At the time of presentation, the lesions in the splenium of the corpus callosum and bilateral cerebral white matter showed diffusion restriction with reduced apparent diffusion coefficient and no reduction in fractional anisotropy (FA) values on diffusion tensor imaging (10). On follow-up, diffusion restriction completely resolved with normalization of the apparent diffusion coefficient (10). The normal to slightly increased FA values in the lesions may indicate that MERS is a non-degenerative disorder (10). The reversible lesion was present for 5–7 days. Our patient suffered from MERS, but the T2 hyperintense lesion was present for 2 months, moreover not only SCC was affected.

Reversible splenial syndrome of the corpus callosum (RESLES) belongs to a new clinico-radiological diagnosis. Its development is attributed to antiepileptic drugs, alcohol abuse, hypernatremia, altitude sickness, radiation therapy, various toxic exposures, and infectious agents (2, 3). The etiology of MERS is infectious (1, 12), which was present also in our patient.

Reversible lesions in the splenium of the corpus callosum (SCC), caused by various infective agents such as influenza, rotavirus, mumps, Escherichia coli, and adenoviruses, have been documented in the literature. The changes

Tab. 1: Clinical conditions associated with splenial hyperintensity.

Possible pathological causes	Disorders
Infections	Encephalitis Malaria Salmonella Rotavirus
Epilepsy	Seizures AED overdose Abrupt drug withdrawal
Demyelinating diseases	Multiple sclerosis ADEM NMO
Vascular diseases	Ischemic stroke Hypertensive encephalopathy Post-cardiac arrest PRES Migraine with aura
Metabolic	Hypoglycemia Hyper/hyponatremia Renal failure
Miscellaneous	Drug toxicity (cyclosporine, fluorouracil) High-altitude cerebral edema Trauma – diffuse axonal injury Malnutrition – Vitamin B12 deficiency

AED antiepileptic drugs
ADEM acute disseminated encephalomyelitis
NMO neuromyelitis optica
PRES posterior reversible encephalopathy syndrome

become apparent on MRI as early as the second day of onset of symptoms, and CSF findings are usually normal or non-specific (4).

Many hypotheses have been suggested to explain such transient lesions of the SCC. Reversible demyelination due to antiepileptic drugs like primidone or carbamazepine may reduce arginine vasopressin levels, with changes of osmolality. According to another hypothesis, viral antigens or antibodies have an increased affinity for the receptors on splenial axons, resulting in inflammatory infiltrates. In 2003, Oster et al. reported reduced apparent diffuse coefficient (ADC) values in a reversible splenial lesion, seen on MRI (6). They suggested that repeated and excessive electrical discharges along the commissural fibers during seizures had caused transient changes in energy metabolism and ionic transport, resulting in rapidly resolving intramyelinic edema. We agree that the SCC is a specific anatomical structure with predisposition to edema, toxic changes of myelin, and vascular changes with hypoxia and ischemia.

Differential diagnosis associated with splenium abnormalities includes: Marchiafava-Bignami Syndrome, renal failure, metabolic abnormalities (mainly sodium and glucose level disturbances), encephalitis from influenza or rotavirus infection, altitude sickness, intoxication, antiepileptic drug treatment, thiamin deficiency, and alcoholism. Presumably, all of these conditions can disturb cellular fluid regulation and lead to a cellular lesion (9).

Conclusion

Transient hyperintense T2 MRI lesion in the middle of the splenium of the corpus callosum is associated with confusion, epileptic seizures, and mental changes. The etiology of the lesion is varied – toxic, hypoxic, and inflammatory – and its duration is 1–2 weeks. We have described a case of a young man with fever, meningeal syndrome, and confusion. We think the cause was viral encephalitis. It is unique because the clinical findings and the MRI lesion were present for two months. In addition, they were associated with optic nerve edema and urinary retention. Over a period of seven months, all the findings have improved, and the patient is now able to work full-time and engage in sports again.

References

1. Degirmenci E, Degirmenci T, et al. Mild encephalitis/encephalopathy with a reversible splenial lesion (MERS) in a patient presenting with papilledema. Acta Neurol Belg 2015 Jun; 115(2): 153–5.
2. Ehler E, Latta J, Eichlerová A, Mrklovský M, Urban P. Exposure of iodomethane and dichlomethane associated with a confusional state. Neurotoxicology 2011; 32: 307–311.
3. Garcia-Monco JCI, Cortina IE, Ferriera E, Martinez A, Ruiz L, Cabrera A, Beldarrain MG. Reversible splenial lesion syndrome (RESLES): what's in a name? J Neuroimaging 2011 Apr; 21(2): e1–14.
4. Kazi AZ, Joshi PC, Kelkar AB, Mahajan MS, Ghawate AS. MRI evaluation of pathologies affecting the corpus callosum: A pictorial essay. Ind J Radiol Imag 2013; 23(4): 321–332.
5. Matthew T, Badachi S, Sarma GRK, Nadig R. "Boomerang sign" in rickettsial encephalitis. Neurology India 2014; 62(3): 336–338.
6. Oster J, Doherty C, Grant PE, Simon M, Cole AJ. Diffusion-weighted imaging abnormalities in the splenium after seizures. Epilepsia 2003; 44: 852–854.
7. Park, MK, Hwang SH, Jung S. Lesions in the splenium of the corpus callosum: clinical and radiological implications. Neurology Asia 2014; 19: 79–88.
8. Polster T, Hoppe M, Ebner A. Transient lesion in the splenium of corpus callosum: three further cases in epileptic patients and a pathophysiological hypothesis. J Neurol Neurosurg Psychiatry 2001; 70: 459–463.
9. Rocha AJ, Reis F, Gama HPP. Focal transient lesion in the splenium of the corpus callosum in three non-epileptic patients. Neuroradiology 2006; 48: 731–735.
10. Shankar B, Naravanan R, Muralitharan P, Ulaganathan B. Evaluation of mild encephalitis/encephalopathy with a reversible splenial lesion (MERS) by diffusion-weighted and diffusion tensor imaging. BMJ Case report, published online 4 June 2014, doi: 10.1136/bcr-2014–204078.
11. Takanashi JI, Shiihara T, Hasegawa. Clinically mild encephalitis with a reversible splenial lesion (MERS) after mumps vaccination. J Neur Sci 2015; 349(1–2): 226–8.
12. Takayuki O, Yasuyuki S, et al. Clinically mild encephalitis/encephalopathy with a reversible splenial lesion associated with febrile urinary tract infection. Eur J Pediatr 2014; 173(4): 533–536.

Received: 14/05/2015
Accepted in revised form: 10/09/2015

Corresponding author:

MUDr. Alena Meleková, Department of Neurology, Hospital of the Pardubice Region, Kyjevská 44, Pardubice 532 03, Czech Republic; e-mail: alena.melekova@nemocnice-pardubice.cz